The influence of adhesion molecules on binding and protein organization in cell contacts

Dam, Tommy

2022

Document Version:
Peer reviewed version (aka post-print)

The influence of adhesion molecules on binding and protein organization in cell contacts

TOMMY DAM | DIVISION OF PHYSICAL CHEMISTRY | LUND UNIVERSITY

The influence of adhesion molecules on binding and protein organization in cell contacts

The influence of adhesion molecules on binding and protein organization in cell contacts

By
Tommy Dam

LUND
UNIVERSITY

DOCTORAL DISSERTATION

Doctoral dissertation for the degree of Doctor of Philosophy (PhD) at the Faculty of Science at Lund University to be publicly defended on the 14th of December at 13.00 in Lecture Hall A, Department of Chemistry, Naturvetarvägen 14, Lund, Sweden

Faculty opponent
Prof. Anton van der Merwe

Organization LUND UNIVERSITY	**Document name** DOCTORAL DISSERTATION
	Date of disputation 2022-12-14
Author(s) Tommy Dam	Sponsoring organization

Title and subtitle

The influence of adhesion molecules on binding and protein organization in cell contacts

Abstract

Interactions between immune cells such as T cells and antigen-presenting cells (APCs) are integral for mounting an adaptive immune response. The interaction between the T cell receptor (TCR) and the antigen-presenting major histocompatibility complex (pMHC) on a contacting T cell and APC, is widely accepted to be the key interaction. If the interaction is favourable, then T cell activation occurs. A large pool of research has been aimed at characterizing this interaction by measuring the binding kinetics and relating it to the T cell response. A simplified model membrane system called a supported lipid bilayer (SLB) is often used to mimic the membrane of the APC.

In many T cell activation studies, the SLB contains the nickel-chelating lipid DGS-NTA(Ni) to functionalize the SLB with histidine-tagged proteins. In the first part of this thesis I show that interactions between DGS-NTA(Ni) and the T cells can lead to, unwanted, T cell signaling. It was found that increasing the concentration of DGS-NTA(Ni) both increased cell adhesion and the fraction of signaling cells. Adding bovine serum albumin (BSA) functioned as a blocking agent, preventing unspecific cell adhesion and decreased the fraction of signaling cells down to a basal level. A low level of signaling was also obtained when functionalizing the blocked SLBs with adhesion molecules binding to receptors on the T cell. In contrast, without blocking these functionalized SLBs again signaled at a similar level to the unblocked, not functionalized DGS-NTA(Ni) SLBs. The DGS-NTA(Ni) signaling was argued to be due to TCR-DGS-NTA(Ni) interactions and stressed the importance of adequately blocking these interactions in T cell activation studies.

In the second part of the thesis, a new method to measure the two-dimensional dissociation constant (2D Kd) of ligand-receptor interactions on single cells is presented. This is measured on individual cell-SLB contacts, providing an accurate new means of measuring binding affinity and to study differences in the 2D Kd in the cell population. In the final part of the thesis, the interaction of TCR-pMHC in the presence of adhesion molecules of different length and density is studied. Adhesion molecule pairs of similar height as TCR-pMHC have been argued to facilitate the TCR-pMHC interaction by physically keeping the opposing membranes at an optimal distance for binding. However, adhesion pairs of different height than that of TCR-pMHC are also important for cell-cell contact formation and have been shown to result in an impaired T cell response if removed. To better understand how, and if, adhesion molecules of different lengths influences TCR-pMHC binding the 2D Kd of TCR-pMHC in the presence of differently-sized adhesion molecules was studied. For this purpose, a SLB functionalized with TCR and an adhesion ligand, was allowed to bind cell with pMHC and the corresponding adhesion receptor. It was found that the 2D Kd of the TCR-pMHC interaction could be up to an order of magnitude higher (weaker) than the corresponding value for TCR-pMHC alone when having height-mismatched molecules. In addition, the TCR-pMHC distributed non-homogeneously in the cell-SLB contacts when having height-mismatched adhesion molecules, but homogeneously when having height-matched adhesion molecules. Furthermore, even for height-matched adhesion molecules the 2D Kd of the TCR-pMHC interaction was found to be dependent on the relative density fraction of TCR to adhesion molecules, with low fractions of TCR molecules giving 2-3 times weaker binding. This indicates that TCR-pMHC binding in cell contacts depends significantly on the local environment and not only on the protein-protein interaction per se.

Key words T cell, SLBs, Calcium Signaling, TIRF microscopy, Two-Dimensional affinity, Protein Segregation, Protein Organization, Protein Height

Classification system and/or index terms (if any)

Supplementary bibliographical information		**Language** English
ISSN and key title		**ISBN** 978-91-7422-920-2
Recipient's notes	**Number of pages** 148	Price
	Security classification	

Signature 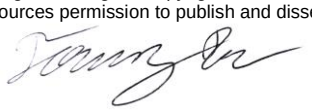 Date 2022-11-01

The influence of adhesion molecules on binding and protein organization in cell contacts

By

Tommy Dam

LUND
UNIVERSITY

Coverphoto by Tommy Dam (made using Blender)

Faculty of Science
Department of Chemistry

ISBN (Print): 978-91-7422-920-2
ISSN (PDF): 978-91-7422-921-9

Printed in Sweden by Media-Tryck, Lund University
Lund 2022

Table of Contents

List of Publications

The work presented in this thesis is based on the following publications, which will be referred to by their roman numerals:

I **Calcium signaling is induced by binding to nickel-chelating lipids in supported lipid bilayers**

Tommy Dam, Victoria Junghans, Jane Humphrey, Manto Chouliara, Peter Jönsson

Frontiers in Physiology, 11:613367, 2021.

II **Single-Cell Measurements of Two-Dimensional Binding Affinity Across Cell Contacts**

Manto Chouliara, Victoria Junghans, Tommy Dam, Ana Mafalda Santos, Simon J. Davis, Peter Jönsson

Biophysical Journal, 120, 5032–5040, 2021.

III **Height mismatched auxiliary molecules significantly reduces binding affinity in cell contacts and influences protein organization**

Tommy Dam, Manto Chouliara, Victoria Junghans, Ana Mafalda Santos, Simon J Davis, Peter Jönsson

Manuscript

The publications are appended at the end of the thesis.

Authors Contribution

I **Calcium signaling is induced by binding to nickel-chelating lipids in supported lipid bilayers**

I did all the experiments with supervision and discussions from Victoria Junghans, Peter Jönsson and Jane Humphrey. I did the analysis of the calcium signaling data with help from Manto Chouliara and Peter Jönsson. Writing was done by me, Peter Jönsson and Victoria Junghans.

II **Single-Cell Measurements of Two-Dimensional Binding Affinity Across Cell Contacts**

Manto Chouliara did the imidazole-related experiments included in the paper while I did the classical Zhu-Golan experiments for the rCD2/rCD48 interaction for comparison with the imidazole-based method. I also did the cell culturing during the project. I contributed with feedback during the writing process.

III **Height mismatched auxiliary molecules significantly reduces binding affinity in cell contacts and influences protein organization**

I did all the experiments included in the ms with supervision from Peter Jönsson. I did the cell culturing, the analysis, wrote the ms, and made the figures.

Publications not included in this thesis:

Supported lipid bilayers and the study of two-dimensional binding kinetics

Tommy Dam, Manto Chouliara, Victoria Junghans, Peter Jönsson

Frontiers in Molecular Biosciences, 9, 833123, 2022.

Effects of a local auxiliary protein on the two-dimensional affinity of a TCR-peptide MHC interaction

Victoria Junghans, Manto Chouliara, Ana Mafalda Santos, Deborah Hatherley, Jan Petersen, Tommy Dam, Lena M Svensson, Jamie Rossjohn, Simon J Davis, Peter Jönsson

Journal of Cell Science, 133(15), jcs245985, 2020.

Lipid Bilayer-like Mixed Self-Assembled Monolayers with Strong Mobility and Clustering-Dependent Lectin Affinity

Sing Yee Yeung, Yulia Sergeeva, Tommy Dam, Peter Jönsson, Guoping Pan, Vivek Chaturvedi, Börje Sellergren

Langmuir 35(24). p.8174-8181, 2019.

Reversible Self-Assembled Monolayers with Tunable Surface Dynamics for Controlling Cell Adhesion Behavior

Sing Yee Yeung, Yulia Sergeeva, Guoqing Pan, Silvia Mittler, Thomas Ederth, Tommy Dam, Peter Jönsson, Zahra El-Schich, Anette Gjörloff Wingren, Adam Tillo, Sabrina Hsiung Mattisson, Bo Holmqvist, Maria M. Stollenwerk, and Börje Sellergren

ACS Appl. Mater. Interfaces 2022, 14, 37, 41790–41799.

List of Abbreviations

2D	Two Dimensional
3D	Three Dimensional
AF	Alexa Fluor
APC	Antigen Presenting Cell
BSA	Bovine Serum Albumin
CCD	Charge-Coupled Device
CD	Cluster of Differentiation
cSMAC	Central Supramolecular Activation Cluster
D	Diffusion constant
DGS-NTA(Ni)	1,2-dioleoyl-sn-glycero-3-[(N-(5-amino-1-carboxypentyl)iminodiacetic acid)succinyl] (nickel salt)
FRAP	Fluorescence Recovery After Photobleaching
FRET	Förster Resonance Energy Transfer
GPI	Glycosylphosphatidylinositol
His-Tag	Histidine Tag
ICAM	Intercellular Adhesion Molecule
Ig	Immunoglobulin
ITAM	Immunoreceptor Tyrosine-based Activation Motifs
K_d	Dissociation Constant
LcK	Lymphocyte-Specific Protein Tyrosine Kinase
LFA	Lymphocyte Function-Associated Antigen
MC	Monte Carlo
MD	Molecular Dynamics
MHC	Major Histocompatibility Complex
NA	Numerical Aperture

NTA	Nitrilotriacetic acid
pSMAC	Peripheral Supramolecular Activation Cluster
RBC	Red Blood Cell
rCD2	rat CD2
rCD48	rat CD48
sCMOS	Scientific Complementary Metal-Oxide Semiconductors
SLB	Supported Lipid Bilayer
SPR	Surface Plasmon Resonance
SUV	Small Unilamellar Vesicle
TCR	T-cell Receptor
TIRF	Total Internal Reflection Fluorescence
TPEM	Two-Photon Excitation Microscopy
ZAP-70	Zeta-chain associated protein 70

Abstract

Interactions between immune cells such as T cells and antigen-presenting cells (APCs) are integral for mounting an adaptive immune response. The interaction between the T cell receptor (TCR) and the antigen-presenting major histocompatibility complex (pMHC) on a contacting T cell and APC, is widely accepted to be the key interaction. If the interaction is favourable, then T cell activation occurs. A large pool of research has been aimed at characterizing this interaction by measuring the binding kinetics and relating it to the T cell response. A simplified model membrane system called a supported lipid bilayer (SLB) is often used to mimic the membrane of the APC.

In many T cell activation studies, the SLB contains the nickel-chelating lipid DGS-NTA(Ni) to functionalize the SLB with histidine-tagged proteins. In the first part of this thesis I show that interactions between DGS-NTA(Ni) and the T cells can lead to, unwanted, T cell signaling. It was found that increasing the concentration of DGS-NTA(Ni) both increased cell adhesion and the fraction of signaling cells. Adding bovine serum albumin (BSA) functioned as a blocking agent, preventing unspecific cell adhesion and decreased the fraction of signaling cells down to a basal level. A low level of signaling was also obtained when functionalizing the blocked SLBs with adhesion molecules binding to receptors on the T cell. In contrast, without blocking these functionalized SLBs again signaled at a similar level to the unblocked, not functionalized DGS-NTA(Ni) SLBs. The DGS-NTA(Ni) signaling was argued to be due to TCR-DGS-NTA(Ni) interactions and stressed the importance of adequately blocking these interactions in T cell activation studies.

In the second part of the thesis, a new method to measure the two-dimensional dissociation constant (2D K_d) of ligand-receptor interactions on single cells is presented. This is measured on individual cell-SLB contacts, providing an accurate new means of measuring binding affinity and to study differences in the 2D K_d in the cell population. In the final part of the thesis, the interaction of TCR-pMHC in the presence of adhesion molecules of different length and density is studied. Adhesion molecule pairs of similar height as TCR-pMHC have been argued to facilitate the TCR-pMHC interaction by physically keeping the opposing membranes at an optimal distance for binding. However, adhesion pairs of different height than that of TCR-pMHC are also important for cell-cell contact formation and have been shown to result in an impaired T cell response if removed. To better understand how, and if, adhesion molecules of different lengths influences TCR-pMHC binding the 2D K_d of TCR-pMHC in the presence of differently-sized adhesion molecules was studied. For this purpose, a SLB functionalized with TCR and an adhesion ligand, was allowed to bind cell with pMHC and the corresponding adhesion receptor. It was found that the 2D K_d of the TCR-pMHC interaction could be up to an order of magnitude higher (weaker) than the corresponding value for

TCR-pMHC alone when having height-mismatched molecules. In addition, the TCR-pMHC distributed non-homogeneously in the cell-SLB contacts when having height-mismatched adhesion molecules, but homogeneously when having height-matched adhesion molecules. Furthermore, even for height-matched adhesion molecules the 2D K_d of the TCR-pMHC interaction was found to be dependent on the relative density fraction of TCR to adhesion molecules, with low fractions of TCR molecules giving 2-3 times weaker binding. This indicates that TCR-pMHC binding in cell contacts depends significantly on the local environment and not only on the protein-protein interaction per se.

Populärvetenskaplig sammanfattning

Varje sekund står vår kropp under angrepp mot smittoämnen såsom bakterier, virus, och parasiter. Men ofta lyckas vi hålla oss friska tack vare vårt immunförsvar. Immunförsvarets jobb sköts av immunceller där T celler har en speciellt viktig roll. T cellen kan känna igen smittoämnen via en speciell molekyl som kallas för T-cellreceptorn och sedan eliminera en infekterad cell eller hjälpa andra immunceller genom att koordinera en attack mot smittoämnet. Mer direkt så växelverkar T-cellreceptorn med små delar av smittoämnet som brutits ner av så kallade antigenpresenterande celler och som sedan just presenteras på ytan av dessa celler som del av ett större molekylkomplex som kort går under namnet pMHC. Olika studier har argumenterat för att det är hur starkt T-cellreceptorn växelverkar med pMHC som avgör om T cellen aktiveras eller inte. För att kunna studera växelverkan mellan TCR och pMHC brukar man ofta ersätta en av de två växelverkande cellerna med ett modellsystem med en känd, enklare sammansättning. Ett av de mer populära modellsystemen är så kallade 'supported lipid bilayers', eller förkortat SLBs, som i princip fungerar som ett cellmembran vilande på en underliggande glasyta, men där sammansättning är känd och välkontrollerad.

Jag visar i den första delen av avhandlingen att även om SLBer gör det möjligt att i detalj studera växelverkan mellan protein som T-cellreptorn och pMHC, och hur detta kopplar till T cellers förmåga att aktiveras, så kan också T celler aktiveras ospecifikt genom att växelverka med andra molekyler i SLBet. Speciellt är det en vanligt förekommande molekyl i SLBet som går under namnet DGS-NTA(Ni) som kan åstadkomma detta. Det är därför viktigt att undertrycka denna molekyl för att inte oavsiktligt aktivera T celler som binder till bilagret, något som jag visade kan göras genom att sätta till bovint serumalbumin till provet.

I den andra delen av avhandlingen presenterar jag en ny metod för att kunna kvantifiera växelverkan mellan bindande molekyler, som T-cellreceptorn och pMHC, i cellkontakter. Denna metod mäter andelen av molekyler som är bundna i en kontakt mellan ett SLB (innehållande den ena molekylen) och en cell (innehållande den andra molekylen) och kan i motsats till tidigare metoder göra detta på enskilda celler. Detta är viktigt, dels för att det visade sig göra metoden mer känslig, men också för att man på detta vis kan studera hur växelverkan variera mellan olika celler.

Slutligen visar jag att växelverkan mellan T-cellreceptorn och pMHC också beror på andra bindande molekyler i cellkontakten och speciellt hur höga dessa molekyler är i förhållande till T-cellreceptor-pMHC komplexet. För att studera detta användes SLBer innehållande både T-cellreceptorer och hjälpmolekyler av olika höjd. Slutsatsen var att om dessa hjälpmolekyler har en total höjd som motsvarar T-cellreceptor-pMHC komplexet så hjälper det till att bilda cellkontakter och T-cellreceptor-pMHC växelverkar optimalt. Om å andra sidan hjälpmolekylerna är

mindre eller högre, och här räcker det med ett par enstaka nm, så växelverkar T-cellreceptor-pMHC avsevärt svagare, och de olika molekylerna fördelar sig också ojämnt i cellkontakten. Att växelverkan mellan T-cellreceptorn och pMHC kan påverkas så märkbart av vilka andra molekyler som finns på cellytan visar på en ytterligare komplexitet i dessa interaktioner som ofta försummats men som kan vara viktiga för att bättre förstå hur T celler aktiveras.

Aim of the thesis

The molecular mechanism initiating T cell activation does not solely revolve around the TCR-pMHC interaction but rather involves a large variety of membrane proteins. Adhesion molecules, costimulatory molecules and coreceptors can greatly affect the outcome. But how the interplay of these protein affects the resulting T cell activation is not fully known and as a consequence the T cell activation mechanism is still unresolved. To shed a light on this, T cells are often used together with protein-functionalized model membrane systems to approximate an opposing membrane surface. However, recent studies have shown that T cells can seemingly undergo early stages of activation in the absence of a TCR-pMHC interaction when interacting with these model membrane systems. The first aim of this thesis was therefore dedicated towards understanding how these protein-funtionalized model membranes (Paper I) can initiate the early stages of T cell activation. Such understanding would be helpful when trying to avoid unspecific signaling events when using model membranes in cell activation studies. In addition, understanding how these signaling events occur could shed some light onto the requirements for initiating a signaling event *in vivo*.

It is generally accepted that the full activation of T cells is regulated by the TCR-pMHC interaction. For this reason, many studies have aimed at characterizing this interaction under various conditions. Characterizing a protein-protein interaction is commonly done by measuring the binding affinity. However, measuring this parameter when the proteins are anchored in a two-dimensional (2D) membrane environment has proven difficult and only a few techniques exist for measuring this parameter. As a consequence, we developed a new binding affinity assay to measure the 2D binding affinity of a protein-protein interaction (Paper II). This single-cell binding affinity assay was then used to investigate the influence of different adhesion molecules on the binding affinity of TCR-pMHC interactions. Due to the TCR and pMHC being anchored to opposing membranes, the proteins must rely on the intermembrane distance for the opportunity to interact with each other. This distance is largely influenced by the size of other binding molecules in the contact. Adhesion molecules which are of similar size to TCR, such as CD2, are therefore thought to play an essential role as a facilitator of TCR-pMHC interactions by positioning the opposing membranes at am optimal distance for binding. In contrast, longer adhesion molecules are also acting to stabilize cell-cell contacts in vivo, and could then potentially both aid and impair 2D binding of TCR to pMHC. However, biophysical knowledge on how this actually influences the binding affinity of TCR to pMHC is generally lacking. The last part of the thesis was aimed at measuring the 2D binding affinity of the TCR-pMHC interaction as it is affected by the presence and size of adhesion molecules (Paper III).

Acknowledgements

I could not finish this work without the help and support from many people. If I have forgotten to thank you, then I do apologize but just know that you are not out mind.

First and foremost, thank you Peter! I appreciate all the patience, support and your enthusiasm, which was especially appreciated whenever I felt stuck in my research project. It made the work and research a lot more fun. Thank you for being a teacher, supervisor, a mentor and I am happy to have completed this work under your supervision.

Thank you Joakim! Thanks for helping me out by asking how everything is going and being open to discuss statistics and maths whenever I felt I was out of my depth (which was often). It all acted as a starting point for the single-molecule tracking project which I had a lot of fun working on.

Doing this work was made a lot easier by having a good working environment at Physical Chemistry. Thank you Chris W and Maria S for all the technical support and for just all the good conversations. A big thank you to Madeleine, Vicky, Marco, Patrik, Alexandra and Najla for all the fun memories I now have after four years. I appreciate all the fun office conversations, board games, dinners and for listening to my ridiculous stories.

Thank you to all my friends from outside of work who dragged me out of the lab to remind me that there is more to life than working. Thank you to Andreas, Thelma, Hanna S, Elin, Damir and Egil for all the fun that we have had over the years. It feels nice to have completed this work and still have you by my side. Similarly, I am grateful for having met Fanny, Alexander, Hanna H and Emma and for all the fun game board nights and hangouts that took my mind off work.

Finally, a big thank you to the heartwarming support from my family.

1. Introduction to the adaptive immune system

The human body is under constant threat from pathogens in our environment, which may or may not cause a larger infection. To combat the myriad of potential threats, an immune system was evolved. Common enemies such as bacteria and viruses can cause health conditions such as the common cold, tuberculosis or chicken pox if not properly dealt with. However, bacteria and viruses can adapt and change resulting in new variants of previously encountered pathogens or even completely new ones. Our survival therefore hinges on our immune system to be as complex and flexible as possible in its ability to detect any potential pathogenic threats.

The surveillance for potentially harmful pathogens is largely done by white blood cells, including cells called macrophages and dendritic cells. The latter cells can recognize potential harmful pathogens by protein markers that can be characteristic of the pathogen, or not expressed by the body's own cells. The pathogen will be internalized through phagocytosis and broken down intracellularly. The cells have the ability to display peptide fragments of what was digested. This is done by breaking down the internalized proteins from the pathogen and loading it on a molecular complex called the major histocompatibility complex (MHC), which is then transported to the membrane of the cell. The peptide fragment is referred to as an antigen and needs to be presented to a T cell for a decision of whether the presented antigen is recognized as part of something harmful. For this reason, cells such as dendritic cells and macrophages are also referred to as antigen-presenting cells (APCs). The T cells are lymphocytes and, before any pathogen has been detected, are predominantly situated in the lymphatic system. Once APCs have internalized a pathogen and presented an antigen on its surface, it migrates towards the lymph nodes to present the antigen to the T cells (Figure 1).

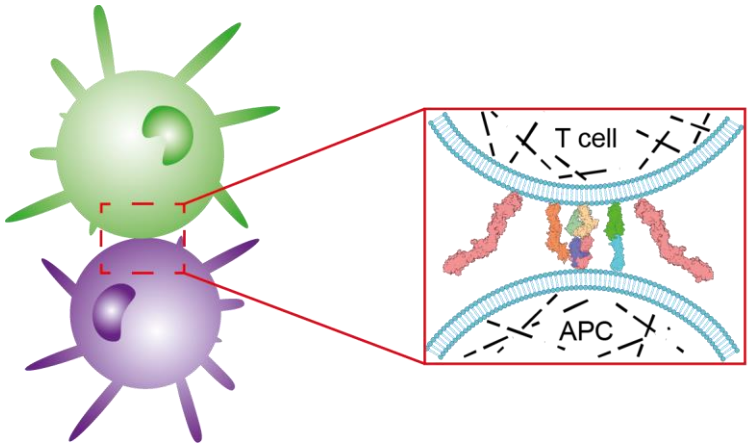

Figure 1.1: A schematic representation of a T cell (green) – APC (purple) contact.
This cell-cell interaction is facilitated by a variety of receptors and ligands (protein structures in the red square), including different signaling molecules, adhesion molecules, coreceptors and membrane-bound enzymes.

Antigen recognition by T cells is accomplished by the expression of the T cell receptor (TCR) on the membrane which binds the peptide-bound MHC complex (pMHC). There are billions of T cells in our bodies and each T cell has approximately 30 000 identical TCRs which recognizes a specific pMHC (1). This gives rise to a large repertoire of cells, each capable of recognizing a unique antigen. Successful antigen recognition by a T cell results in the initiation by an immune response in a process called T cell activation (see chapter 5 for more details). T cell activation can also occur when an intracellular pathogen has been detected. Most of the body's own cells are capable of presenting peptide fragments, onto MHC, from proteins within the cell. These naturally occurring peptide fragments from the cell are referred to as self-peptides and interactions between a TCR and MHCs bound to self-peptides do not, normally, result in antigen recognition. However, in the presence of an intracellular pathogen (such as a virus) a non-self peptide is presented which can lead to T cell activation upon successful antigen recognition with a T cell.

The molecular machinery initiating successful T cell antigen recognition and T cell activation is complex and involves, aside from TCRs and pMHCs, a rich variety of other membrane proteins. Understanding how these proteins interact with each other is crucial for understanding how T cell activation is initiated and modulated, but also for characterizing the cause behind immunodeficient ailments and diseases. A brief description of a few important membrane proteins involved in initiating T cell activation that has been studied in this thesis, is given below.

1.1. Membrane proteins involved in T cell activation

Part of the aim of this thesis is to characterize the interactions between the molecules presented below in order to better understand how they can influence T cell activation. Therefore, a short description of various membrane proteins, as pertained to this thesis, is given below.

1.1.1 The T cell receptor and the major histocompatibility complex

The T cell's ability to recognize specific antigens is due to the TCR that is expressed on the cell membrane. In 95% of T cells this membrane protein is composed of two protein chains, denoted as TCRα and TCRβ respectively, that are bound together by a disulfide bond (1). The remaining 5% of T cells express a type of TCR called γδTCRs (2) which has a not fully understood function but is suspected to recognize phosphoantigens i.e. phosphorylated non-peptide molecules that are essential in the signaling pathways of bacteria, fungi and parasites (3). However, the focus of this thesis will concern T cells expressing αβTCR which will henceforth be referred to as TCR. The TCR bears many structural similarities to antibodies. Like antibodies, both TCRα and TCRβ have a region that resemble the constant region of an antibody and a variable region that forms a highly specific binding site for an antigen (4). The ligand for the TCR is a peptide fragment of a protein that has been processed by an APC and presented on the cell surface. This is accomplished by presenting the peptide via MHC. It is important to note that the TCR recognizes a 'compound' ligand i.e. it does not recognize the antigen alone, rather it needs to be attached to MHC. As such the ligand for TCR is said to be the peptide-loaded MHC (pMHC).

Each unique TCR is not represented by a single gene, rather the T cell undergoes gene rearrangement during early stages of cell development. This results in a large variety of different TCRs from a small set of genes. Furthermore, during development each T cell undergoes strict control measures to ensure that the TCRs are functional, i.e. they can recognize pMHC, but also that they do not recognize pMHC with self-peptides too strongly. This prevents having T cells that could cause autoimmune responses or eliciting too strong immune responses towards a pathogen that could also harm the body. Any T cell that exhibits these traits receives a termination signal and is eliminated from the pool of T cells available for antigen recognition (1, 5).

The source of the presented peptide fragment can either be extracellular or intracellular, each type is attached to a specific class of MHC molecules. Intracellular peptides are presented by MHC class I while extracellular derived peptide fragments are loaded onto MHC class II. With the exception of red blood cells, all cells express MHC class I whereas antigen-presenting cells (B cells, dendritic cells and macrophages etc.) also express MHC class II.

1.1.2 The CD2-CD58 adhesion pair

CD2 is a heavily glycosylated adhesion protein expressed on the surface of T cells and NK cells. Its extracellular domain is approximately 8 nm, which is unusually small compared to other adhesion proteins such as integrins (6). The binding site is located on the membrane-distal end where its ligand, CD58, can bind (7, 8). Its rat analogue, rat CD2 (rCD2), binds to rat CD48 (rCD48). CD2 is a well studied protein and its binding affinity has been measured in solution. These studies reveal that the CD2-CD58 interaction is weak (three-dimensional dissociation constant (3D K_d) of 10-20 μM for CD2-CD58 and 60-90 μM for rCD2-rCD48) with a fast dissociation rate (9–11).

Although CD2 might not be vital for T cell activation, at least for mice since mice that do not express CD2 are still able to have functioning immune system (6), it has been shown that CD2 still enhances antigen recognition by facilitating TCR-pMHC interactions (6, 7, 12). By blocking CD2 it was found that cell adhesion to APCs and target cells was impaired and antigen recognition was diminished (7, 12). One property of the CD2 protein that enables it to support TCR-pMHC interactions is its similar size to TCR. As it anchors the opposing membrane by binding to CD58, a membrane gap of approximately 14 nm is created (10, 13, 14). Such distances is similar to the dimensions of the TCR-pMHC binding pair and it is thus believed that this close membrane approximation optimizes the interaction between the two proteins (11, 15).

1.1.3 CD45

CD45 is a transmembrane glycoprotein belonging to the protein tyrosine phosphatase family and is involved in cell signaling and cell differentiation in several different cell types (16). The protein is composed of two tandem intracytoplasmic domains, a transmembrane domain and large, heavily glycosylated, extracellular domain ending in a mucin-like region. The protein is expressed on most immune cells and while the function of CD45 is the same across these cells, the isoform of CD45 will differ depending on cell type and the stage of differentiation. The various isoforms vary in the level of glycosylation as well as the overall length of the mucin-like region, which means the extracellular domains have different dimensions depending on the isoform (16, 17). By using techniques such as hydrodynamic trapping, the height of CD45RABC was measured to be approximately 22 nm (18), which is relatively large compared to other receptors such as TCR, CD2 and CD4. Furthermore, CD45 is well-expressed on T cells and cover approximately 10 % of the cell surface area (19). Together with the heavily glycosylated extracellular domain, this makes CD45 a major component of the glycocalyx – a layer of sugar-coated lipids and proteins that cover the cell membrane

acting as a protective barrier against mechanical shear forces and unwanted contact but also as a scaffold for adhesion proteins (18, 20).

CD45 has both negative and positive effects on T cell signaling. During the initiation stages of T cell activation, called TCR triggering, the TCR is phosphorylated by the lymphocyte-specific protein tyrosine kinase (Lck). CD45 negatively regulates the TCR triggering process by dephosphorylating the TCR complex when interacting with it. However, CD45 is also capable of positively regulating the TCR triggering process by dephosphorylating the negative regulatory C-terminal tyrosine phosphorylation sites of Lck, which activates it and enables it to phosphorylate the TCR complex. How these seemingly opposing influences are balanced, or interplay, to affect the resulting T cell activation is under debate (21, 22).

2. The cell membrane and model membrane systems

2.1 The lipid bilayer

The intracellular components of a cell is enclosed by a roughly 5 nm thick cell membrane. This membrane forms a protective barrier towards the surrounding environment while allowing passive transport of water across the membrane, and selective transport of certain nutrients such as glucose. Cell membranes are mainly composed of membrane proteins, cholesterol and phospholipids. The phospholipids are described as amphiphilic as it has a hydrophilic region (commonly referred to as the head group of the lipid) and a long hydrophobic region which is composed of 18-20 carbon atoms (commonly referred to as tails) (23–25).

In an aqueous environment, the interactions between the hydrophobic regions of phospholipids and water molecules are unfavourable. It drives the phospholipids to organize themselves in a bilayer structure to minimize these interactions (26). In such a structure, two layers of phospholipids are brought together in such a way that the hydrophilic regions of each layer are facing the aqueous environment while the hydrophobic tails of each layer are facing each other. These same forces that drive lipid bilayer formation, also lead to the cell membrane having mechanical properties that allow it to reseal itself when punctured. When the membrane is subjected to a small tear, the hydrophobic tails of the phospholipids are exposed to the water molecules which is an unfavourable interaction. The phospholipids rearrange to repair the lipid bilayer (25).

In addition to the ability to reseal itself, the cell membrane also acts as a flexible 2D fluid. The lipids and proteins are able to move within the plane of the bilayer. This membrane fluidity is important as it allows for change in the distribution of membrane proteins, which is essential for cell signaling and will be further explored later in the thesis. How easy it is for the lipids and proteins to move within the membrane is commonly characterized by a diffusion constant and is largely affected by the membrane composition (27). Phospholipids with longer and saturated hydrophobic tails interact with each other more and can be more packed more tightly in the bilayer. Consequently, a high concentration of these lipids in the cell membrane decreases the fluidity. In contrast, phospholipids with either shorter

hydrophobic tails, or tails containing double-bonds result in a less dense packing of the lipids and therefore increase the fluidity of the membrane (24).

2.2 Supported lipid bilayers

A common model membrane system for the native cell membrane is the supported lipid bilayer (SLB). SLBs are comprised of a lipid bilayer resting on a substrate for support which increases the stability and results in a stable model membrane system over time. Between the SLB and the substrate is a 1-2 nm thick hydration layer which preserves the lateral mobility of lipids (28). The number of lipid species is often reduced to only a few to reduce the complexity of the membrane system (29).

There are a few techniques to accomplish successful SLB formation such as the Langmuir-Blodgett dipping method (30), spin-coating (31) or vesicle rupture and fusion (32, 33). In the spin-coating method the lipid solution is dripped onto a substrate which rapidly spins, causing the solvent (often chloroform) to evaporate and the lipids to distribute evenly over the substrate. A lipid film is formed upon rehydration of the surface. In the Langmuir-Blodgett technique the SLB is built up one monolayer at a time. The monolayers are formed at an air-water interface. The monolayers are then transferred to a substrate by dipping it in and out of the lipid-covered liquid. Dipping the substrate multiple times into the liquid builds up multilayers and more complex lipid structures. The Langmuir-Blodgett technique also allows one to control the lipid composition and symmetry in each individual monolayer. However, it requires more expensive machinery to control the substrate submersion and to get defect-free SLBs (34, 35). A cheaper and more simple method is often used which is the vesicle rupture and fusion method (Figure 2.1). In this method, vesicles with the desired lipid composition are in an aqueous solution above the surface. Due to electrostatic interactions between the substrate and the vesicles, the vesicles adsorb to the surface. At a sufficiently high surface coverage, the vesicles rupture and fuse together to form a 2D lipid bilayer when the density of vesicles is sufficiently large (32, 36, 37). Due to its simplicity, the vesicle rupture and fusion method was used to produce all SLBs used in the experiments presented in this thesis.

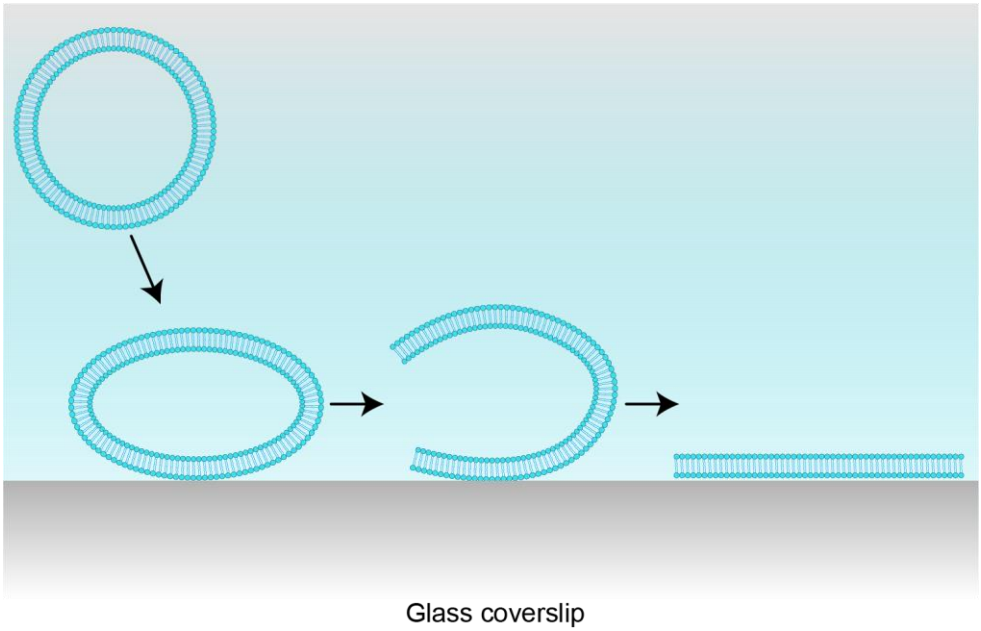

Figure 2.1: Illustration of SLB formation through vesicle rupture and fusion.
SUVs are deposited onto a hydrophilic glass coverslip whereupon the vesicles rupture and fuse to form a continuous 2D lipid bilayer when the surface coverage of vesicles is sufficiently high.

2.2.1 Protein functionalization strategies

Cell studies require functionalizing the SLB with proteins to better resemble native cell membrane. The proteins have to be integrated into the SLB in such a way that the lateral mobility is maintained. However, integrating a whole protein structure into a SLB has proven to be difficult. Integrating proteins with respective ectodomains, transmembrane domain and cytoplasmic domain results in immobility due to interaction with the substrate (38). One solution is to eliminate the substrate altogether as in the case of black lipid bilayers where a bilayer is formed in an aperture of a hydrophobic material. However, the black lipid bilayer is prone to rupturing from small hydrodynamic pressures and incorporating other techniques such as nuclear magnetic resonance and fluorescence microscopy has proven difficult (39, 40). A more widely used solution has been to reconstitute the lipid bilayer with a poly(ethylene glycol) (PEG) spacer which further separates the lipid bilayer from the underlying substrate. Depending on the size of the integrated protein, the gap may need to be increased which can be achieved by increasing the molecular weight of the PEG spacer (41–43). The PEGylated lipids are incorporated into the vesicles themselves when forming an SLB through the vesicle rupture and fusion process (43) and the lipids do not interact with the substrate while still being

capable of providing a steric repulsion which prevents the lipid bilayer from adhering and interacting with it (44).

Since the experimental work in this thesis is mainly concerned with the binding kinetics of membrane proteins, and less with the intracellular molecular mechanisms, only the ectodomains of the proteins of interest are added to the bulk-facing leaflet of the SLB. This can be accomplished by using protein-lipid linkers such as (a) GPI-linkers, (b) His-tagged proteins which binds to nickel-chelating lipids or (c) biotin-streptavidin linked proteins (Figure 2.2).

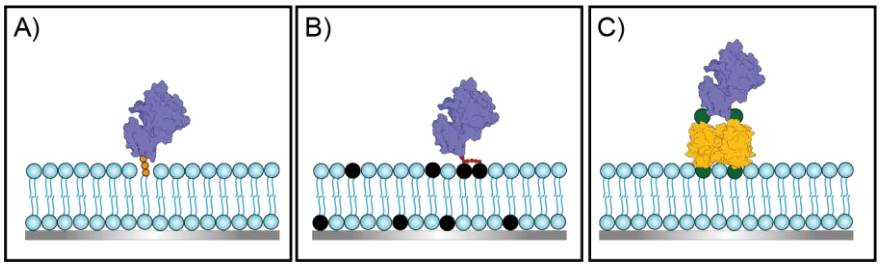

Figure 2.2: Illustrations of three possible protein linkage strategies for SLB systems.
Proteins (purple) can be attached to SLBs via **(A)** a GPI-linker (orange) which covalently attaches the proteins to the lipids, **(B)** via non-covalent bonds between polyhistidine tags (red) and nickel-chelating lipids (lipids with black headgroups) and via **(C)** strong non-covalent biotin- (green) streptavidin (yellow) interactions.

Glycosylphosphatidylinositol (GPI) anchors are posttranslational covalent modifications that results in the attachment of proteins to the outer leaflet of the SLB (Figure 2.2A) (45, 46). In in-vitro experiments the GPI-linked proteins can be incorporated into the SLBs by inserting the GPI-linker into the lipid bilayer. The GPI-linked proteins can be expressed naturally by using E.coli systems or the anchors can be added synthetically to a protein (29). In both cases, the protein purification and membrane preparation step can be complicated (47). Furthermore, the GPI-linker has been shown to induce protein aggregation in certain conditions (48). An alternative is to incorporate nickel-chelating lipids of which DGS-NTA(Ni) is commonly used. Proteins can be attached to the SLBs by conjugating polyhistidine-tags (His-tag) to the protein which leads to binding with the DGS-NTA(Ni) once the lipids have been loaded with Ni^{2+}-ions (Figure 2.2B) (29). This linkage method is convenient and is widely used. However, the interaction between the His-tag and DGS-NTA(Ni) is weak and not covalent as it is in the case of GPI-linked proteins. This leads to a reversible protein functionalization and protein detachment is observed over time. It is therefore recommended to conjugate a His-tag, to the proteins, comprised with at least 10 histidine residues and use longer incubation time for an adequate surface density of proteins (29, 49). The nickel-chelating system can be replaced with the streptavidin-biotin system for a stronger linkage (Figure 2.2C). One drawback, however, is that streptavidin is multivalent which can lead to oligomerization of the functionalized proteins. Furthermore, the

biotin-streptavidin complex is approximately 5 nm in height which also increases the height of any proteins conjugated to the SLB. Depending on the purpose of the experiment, this may be undesirable (47).

To avoid uncontrollable protein aggregation, and due to the interest of investigating the influence of protein size on binding kinetics, DGS-NTA(Ni) were used as the protein-SLB linkage system for all presented work in this thesis. Unless stated otherwise, all SLBs contained POPC and DGS-NTA(Ni)-lipids.

3. Fluorescence microscopy

3.1 The theory behind fluorescence

The development of microscopes has been paramount for the study of cells as it allows the user to visually observe the details of cellular events. To properly view the cells at a sufficient level of detail, it is important to increase the contrast between the signal (the cellular structures) and the background. In that regard, fluorescence microscopy has been an invaluable tool (50).

Fluorescence microscopy hinges on the requirement of attaching fluorescent molecules onto cellular structures of interest. When not illuminated with light the electrons, in the fluorescent molecules, are in what is called a ground state, a lower energy state. However, upon light illumination the electrons can transition to a higher energy state by absorbing the photons (Figure 3.1A). In contrast to many measurable quantities in the macro world, the laws of quantum mechanism dictates that the energy levels available for the electrons are discrete and not continuous. As such, a transition to higher energy states is only possible if the electrons adsorb photons with an energy equal to the energy difference between the ground state and the higher transition state. The energy, *E,* of a photon is linked to its wavelength via Planck's equation:

$$E = h \cdot f = \frac{h \cdot c}{\lambda} \qquad (Eq.\ 3.1)$$

where h is Planck's constant and f is the frequency and λ is the wavelength. Upon absorption, the electrons spend a short amount of time (on the scale of picoseconds) in the higher energy states before via thermal and vibrational relaxation the protein transitions to the lowest excited energy state. Here the electron stays on average for a few nanoseconds before the electron transitions back to the ground state, in the process emitting so called fluorescence light with a lower frequency (energy) than the frequency (energy) of the exciting photon. This difference is commonly referred to as Stokes shift (Figure 3.1B) and is quite useful in microscopy as it allows the user to detect the fluorescent signal due to the fact that excitation light and emitted light have distinct wavelengths (51).

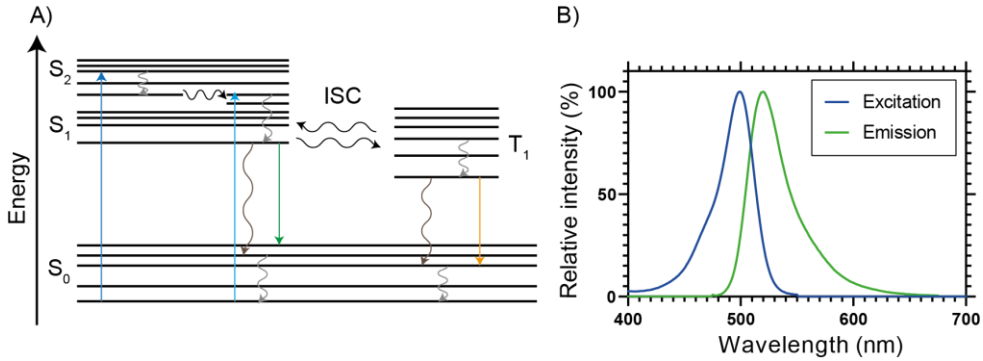

Figure 3.1: (A) A Jablonski diagram illustrating the fluorescence process. Electrons in the ground state (S0) make a transition to higher energy levels (S2) by absorbing photons (blue arrow). Through vibrational relaxation (gray arrow) and internal conversion (black arrow), the electrons can relax down to the lowest excited singlet state (S1). The electron can then return to the ground state through fluorescence by emitting a photon (green arrow), or through non-radiative processes (brown arrow). Another possibility is intersystem crossing (ISC) to a triplet state where the electrons can return to the ground state via phosphorescence (yellow arrow). **(B)** Return to the ground state via fluorescence results in the emission of a photon which has a longer wavelength than the absorbed photon. This difference in wavelength is referred to as Stokes shift.

Instead of a fluorescence emission transitioning the excited electron back to the ground state it is also possible for the electron to do a so called intersystem crossing (ISC) and transition to a triplet state (Figure 3.1A). Triplet states are relatively long-lived as it is more difficult for electrons to transition back to the singlet ground state. In these states, the electrons are therefore more prone to undergo photochemical reactions that causes destruction of the fluorescent molecule, so called bleaching (50, 51).

While bleaching is one of the main drawbacks in fluorescence microscopy, it is essential for the technique fluorescence recovery after photobleaching (FRAP) discussed in section 3.4. In addition, new fluorophores are constantly being developed to have a higher photostability in addition to having brighter fluorescent emissions. Furthermore, the library of available fluorophores is constantly being expanded with new labelling strategies which makes it possible to investigate a larger variety of cellular structures (50).

3.2 The fluorescence microscope

A common configuration of the fluorescence microscope is the epi-illumination, which means that the excitation light and the emitted fluorescence light exits the microscope on the same side (Figure 3.2).

The light source in the setup can vary from arc lamps, lasers to light emitting diodes (LEDs), among others. Each type has its advantages and disadvantages and the choice of light source will depend on which fluorescent probe being used (52). Arc lamps emit light in a broad range of wavelengths, making it compatible with many commonly used fluorophores (51). But to obtain wavelengths in a narrow band requires a series of filters and the lifetime for the light bulb is short which means alignment is required each time the bulb is replaced (52). Lasers produce monochromatic light with high intensity and is compatible with 2D and 3D fluorescent imaging of cells and tissue using techniques such as confocal imaging or two-photon excitation microscopy (TPEM) (51, 52). However, one common issue with using lasers as a light source is the potential for producing diffraction patterns on the image due to dust or other types of interference along the light path (52). Another light source which produces monochromatic light is LED which also consumes less energy and requires less maintenance but can be expensive (51). Excitation filters are often put in front of the light source to further narrow down the bandwidth of wavelengths, and therefore also within a certain energy range, which is required to put the electrons of a fluorophore in an excited state. The light is then led towards the objective which illuminates, as well as magnifies and images, the sample.

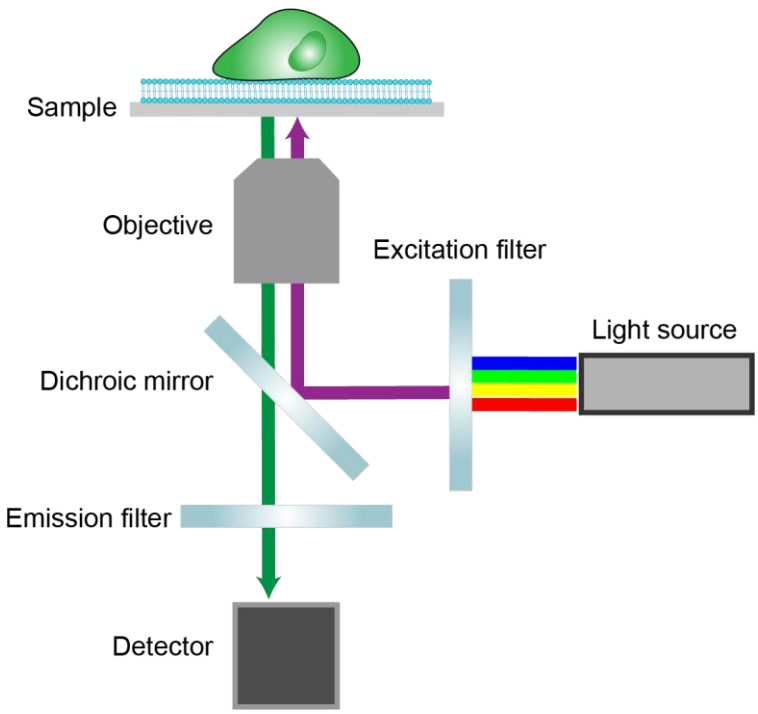

Figure 3.2: A schematic of a general fluorescence microscope setup to illuminate the sample with epi-illumination.

A fraction of the illuminating light is reflected back through the objective along with the fluorescent emission from the sample. Due to the characteristic Stokes shift, there is a difference in wavelength between these two components. A dichroic mirror is first used to coarsely separate the fluorescent emission from the reflected illuminating light (Figure 3.2). An emission filter is then placed after the dichroic mirror to only transmit the emission light onto a detector in a camera. The detector is a 2D array where each cell is known as a pixel and records the number of arrived photons. The number of photons is converted into an electrical signal to produce a digital file which can be visualized. Commonly used detectors in cameras are charge-coupled devices (CCD) and scientific complementary metal-oxide semiconductors (sCMOS). Both have advantages but generally CCDs have a high sensitivity which can be an advantage for capturing low intensity signals whereas sCMOS have faster image acquisition and can thus be used to image rapid events (51, 53).

3.3 TIRF microscopy

A standard epi-fluorescence setup as described in the previous chapter illuminates a large sample volume (Figure 3.3A) which can be undesirable if the object, or event, of interest occurs close to the sample surface. Under these circumstances it is desirable to suppress fluorescent emission originating from the bulk solution to achieve a higher signal-to-noise ratio. For this purpose total internal reflection fluorescence (TIRF) microscopy is a powerful and suitable technique (54, 55). In TIRF microscopy, the excitation light is directed towards the sample above a critical angle, $\Theta_{critical}$, under which the excitation light will undergo total internal reflection rather than passing through the sample (Figure 3.3B).

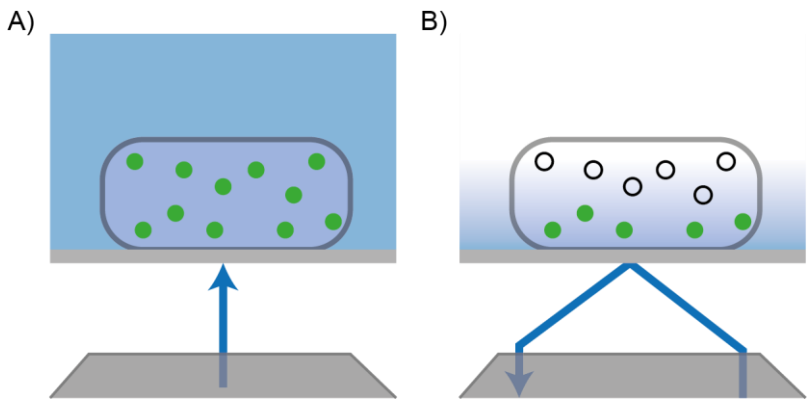

Figure 3.3: Comparison between **(A)** normal epifluorescence illumination and **(B)** TIRF illumination.

The difference in refractive index between the glass coverslip (n_1) and the aqueous solution in the sample (n_2), determines the critical angle (51, 54):

$$\Theta_{critical} = \sin^{-1}(\frac{n_1}{n_2}) \qquad (Eq.\ 3.2)$$

As the excitation light undergoes total internal reflection at the sample surface, a thin electromagnetic wave is generated that decays with distance from the surface. This wave is referred to as an evanescent wave and it has the same frequency as the incident light. One of the advantages of TIRF microscopy is that this evanescent wave decays exponentially with the distance away from the sample surface. The penetration depth, *d*, depends on the two refractive indices, n_1 and n_2, the excitation wavelength, λ_0, and the incident angle, θ, (51, 54):

$$d = \frac{\lambda_0}{4 \cdot \pi}(n_2^2 \sin^2 \theta - n_1^2)^{-1/2} \qquad (Eq.\ 3.3)$$

resulting in a penetration depth that is typically around 100 nm (54). Due to the main research questions in this thesis revolving around measuring binding kinetics of proteins at a cell-SLB interface close to the sample surface, TIRF microscopy was used in all experiments unless stated otherwise.

3.4 Fluorescence recovery after photobleaching

While bleaching of fluorophores is an unwanted process that limits the observation time of fluorophores, the property is used to advantage in the technique FRAP. In this method, the fluorescently labelled components of a lipid bilayer are subjected to a high intensity light pulse within a confined area (Figure 3.4A). This results in bleaching of the labelled components in the area which is observed as a black region in a fluorescence microscope. The fluorescently labelled molecular species are laterally mobile in the lipid bilayer and will therefore diffuse into the bleached region. As a result, the black region will dissipate as there is an intensity recovery in the area due to an influx of fluorescently labelled species into the bleached region (56–58).

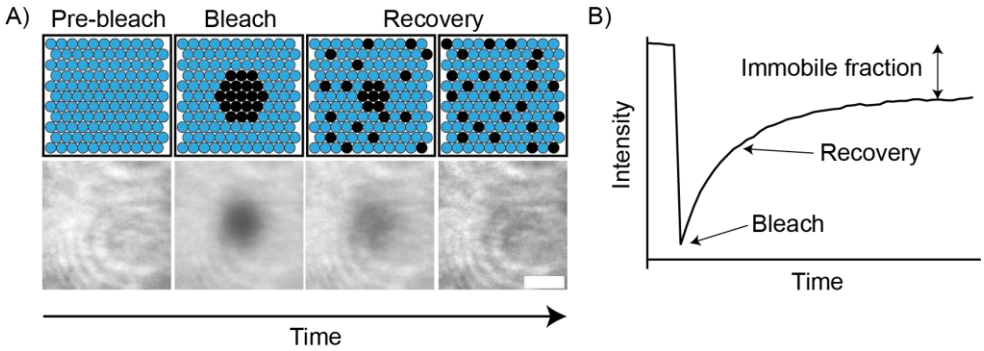

Figure 3.4: (A) A schematic representation of the FRAP procedure for a fluorescently labelled SLB along with representative microscopy images at different stages during the FRAP process. **(B)** The mobility of the fluorescently labelled molecules can be visualized by measuring the mean intensity of the bleached area over time.

The intensity recovery process over time is monitored through image acquisition (Figure 3.4B). The time it takes to recover is related to the mobility of the fluorescently labelled molecules and by fitting this to equations describing the diffusive processes, a diffusion constant, *D*, can be obtained. However, often the intensity does not fully recover back to its starting value due to a fraction of the fluorescently labelled molecules being immobile (Figure 3.4B). This can be due to some lipids or proteins interacting with the underlying substrate through bilayer defects created during SLB formation. When investigating the mobility of molecular species in a native cell membrane, some of the molecular species may also be anchored to the cytoskeleton which hinders their movements. By comparing the fluorescence in the bleached area after the recovery process, with the initial fluorescence, the fraction of immobile molecular species can be obtained (24, 56, 58).

FRAP has become an invaluable method in determining protein- and lipid dynamics in lipid membranes (43, 59, 60). One appeal of the method is that it is relatively non-invasive. The photobleaching process does typically not affect the physical and chemical interactions involving the molecular species in question. Furthermore, the protocol for performing a FRAP measurement is relatively simple. In practice, a low-density neutral density filter in combination with a circular pinhole aperture is placed in front of the light source for high-intensity illumination to cause photobleaching in a delimited area. During image acquisition of the intensity recovery process, the pinhole and low-density neutral density filter is removed and a higher-density neutral density filter is put in place instead to prevent excessive photobleaching during the recovery process. In this work, FRAP was used before each experiment to determine that there was a successful SLB formation.

4. Binding kinetics of receptor-ligand interactions

4.1 A short introduction to receptor-ligand binding kinetics

Proteins are the building blocks of cells and have a variety of functions in our bodies, ranging from transporting oxygen in our blood to catalysing chemical reactions. They are composed of amino acids and each amino acid is characterized by a specific side chain. Interactions between the side chains of each amino acid results in a folded protein structure that determines its function. To perform their functions, a protein needs to bind another molecule. Proteins such as antibodies need to bind bacteria or viruses, motor proteins such as myosin bind actin filaments and enzymes require binding to the substrates that partake in the chemical reaction. The binding is the result of a series of weak non-covalent interactions (e.g. van der Waals interactions, hydrogen bonds or electrostatic interactions). Furthermore, this binding is very specific with every protein only binding up to one or a few proteins out of a myriad of molecules a protein normally encounters in our body (24).

In the context of this thesis, the proteins of interest are signaling- and auxiliary proteins expressed on the membranes of T cells and APCs. The membrane proteins of interest are often referred to as receptors and ligands. Receptor-ligand interactions in the immune system can initiate an immune response, or not, in addition to modulating it. Previous studies have demonstrated that the presence of adhesion molecules on the T cell membrane can increase the antigen sensitivity and facilitate TCR-pMHC interactions respectively. In this thesis, one of the main aims was to investigate how, and what properties of, adhesion molecules influence the binding between TCR and pMHC.

To answer these questions first require a framework of how a receptor-ligand interaction is characterized. One way is by measuring the binding affinity. A receptor-ligand interaction can be described as:

$$[R] + [L] \rightarrow [RL] \qquad (Eq.\ 4.1)$$

where *[R]* is the concentration of free receptors, *[L]* is the concentration of free ligands and *[RL]* is the concentration of formed receptor-ligand complexes. In equilibrium, the affinity constant, K_a is defined as:

$$K_a = \frac{[RL]}{[R][L]} \qquad (Eq.\ 4.2)$$

Another often used parameter is the dissociation constant, K_d which is related to the affinity constant by:

$$K_d = \frac{1}{K_a} \qquad (Eq.\ 4.3)$$

The K_d value has molecular concentration as unit and corresponds to the ligand concentration where half of the receptors are bound. Weaker binding is therefore characterized by a higher K_d value.

While the K_d has been used to characterize complex biological reactions, it is only applicable under equilibrium. Another source of information regarding the binding can be obtained from looking at the on- and off-rates which is linked to the K_d value via:

$$K_d = \frac{k_{off}}{k_{on}} \qquad (Eq.\ 4.4)$$

where k_{off} is the dissociation rate and k_{on} is the association rate. From this expression it is possible to see that multiple receptor-ligand interactions can have the same measured K_d value, but different k_{off} and k_{on} -values. As a result, some bonds can form quickly while others require more time before a strong bond is formed despite having the same K_d. The off rate is in turn inversely proportional to the lifetime of the interaction, which is the average time between bond formation and bond rupture.

4.2 Measuring binding kinetics in 2D

Measuring binding kinetics between ligands and receptors has traditionally been done using solubilised molecules where the receptors have been immobilized on a surface plasmon resonance (SPR) chip. In SPR measurement either the TCR or the pMHC is immobilized on a sensor chip while the other ligand is flowed over the sensor chip in solution. To monitor protein binding a light source illuminates the sample chip at an angle, generating surface plasmons. At a certain resonance angle the adsorption of light is maximum, and this angle depends on the refractive index near the surface of the chip, which is affected by the amount of adsorbed ligands on the surface. As such the change in angle is related to the binding of ligands over time, from which information regarding the binding kinetics can be extracted (61,

62). In general, wild-type TCRs has a low affinity (1-100 μM) and intermediate k_{off} (0.001-0.1 s^{-1}) (63–65) and one of the challenges has been to explain how such weak protein interactions are able to initiate T cell signaling.

However, these SPR measurements yield information about the 3D binding dynamics as one of the binding proteins is freely diffusing in solution. In a native environment, the TCR and pMHC are both membrane-bound proteins and are therefore restricted to a 2D plane. This restriction in movement leads to a difference in diffusion, molecular configuration and ultimately a difference in reaction kinetics which is not captured by binding kinetic measurements in 3D (66). In addition, while many agree on the importance of the TCR-pMHC interaction as a starting point, many have also observed that the resulting T cell response is influenced by the presence of adhesion molecules (10, 67, 68), segregation of membrane proteins (69, 70), the number of presented antigens (71, 72) and the involvement of the cytoskeleton (73). Whereas these effects do not necessarily have to influence the TCR-pMHC binding kinetics investigating whether they do so is not easily demonstrated in a 3D binding affinity assay. To measure more physiologically relevant binding dynamics, binding affinity assays in 2D are needed.

4.2.1 Micropipette-based binding assays

One type of 2D affinity assay is based on bringing the ligands and receptors in periodic contact by using micropipette manipulation of two cells, or a cell and a bead (74). In more detail, receptor-ligand interactions are detected by using a ligand-coated red blood cell (RBC) or ligand-coated bead attached on the RBC. Using a micropipette, the RBC is brought in and out of contact with a cell expressing the corresponding receptor and any ligand-receptor interactions will result in deformation of the RBC as the cells are being pulled away from each other. The RBC and the cell is being brought into contact several times and any adhesion event is recorded to eventually yield an adhesion frequency plot – the likelihood of the ligand interacting with the receptor. From this curve both the effective affinity and the lifetime of the interaction can be obtained. Using this method, it was found that the activation potency of various pMHCs correlated better with 2D lifetimes compared to 3D lifetimes and that these quantities could be orders of magnitude different (73, 75).

One advantage of mechanical-based assays is the ability to study force-dependent protein lifetimes (76). According to Bell the application of force decreases the lifetime exponentially (66). Bonds which express this characteristic is termed slip bonds. In contrast, bonds referred to as catch bonds have been observed to have an increased lifetime when 10-30 pN of force was applied (75). In nature slip bonds are thought to help with cell migration as many bonds are continuously being formed and broken between the surface and the cell as it moves across a surface (77). Catch bonds are instead thought to prolong receptor-ligand interactions and

could therefore play a role in cell signaling and mechanosensing (78, 79). Early investigations into the TCR-pMHC interaction indicated that agonistic pMHC binding TCR show catch bond behaviour while antagonistic pMHC binding TCR showed slip bond behaviour (76, 80, 81). Similar to an early T cell activation model, kinetic proofreading model (82), these results indicated that a difference in lifetime could play a role in the antigen discrimination process. However, other mechanical-based methods such as the flow-chamber method have reported a few exceptions in the 1G4 TCR/HLA-A2 system where agonistic TCR-pMHC interactions do not show ideal catch bond behaviour (83). In the absence of force, a lifetime of 5-10 s was measured but remained unchanged by forces as high as 50 pN indicating ideal bonds (83). It has been argued that catch bond behaviour arise during specific circumstances, such as when the force is applied in a pulling geometry (84).

The micropipette-based assays also has some limitations. The assays are limited to examining one protein-ligand pair at a time, making it difficult to examine the binding kinetics in a more native environment where more than one receptor-ligand interaction type is present (85). Furthermore, the resulting adhesion between two cells is also dependent on the contact area which is not readily measurable in micropipette-based assays, thus only providing an effective K_d value. To fully investigate the influence of force on receptor-ligand interaction requires varying parameters such as the magnitude of force and the loading rate as well as the choice of mechanical-based measuring technique as the properties of the transducer can affect the results as well (86).

4.2.2 Zhu-Golan measurements of 2D binding affinity

Another popular alternative to measure the 2D binding affinity is to use fluorescence-based methods, where the Zhu-Golan methods has proven especially useful (87–90). In this method fluorescently labelled ligands are anchored in an SLB and are allowed to bind to receptors on a contacting cell. This results in an accumulation of ligands in the cell-SLB contact that depends on the 2D K_d of the interaction and the density of ligands and receptors (Figure 4.1A) (91). By varying the ligand density in the SLB and monitoring the relative accumulation of ligands in the cell-SLB contacts the Zhu-Golan expression can be used to determine both the 2D K_d of the ligand-receptor interaction as well as the receptor density on the cells (Figure 4.1B) (87):

$$\frac{B}{F} = \frac{N_t \cdot f}{K_d \cdot S_{cell}} - \frac{B \cdot p}{K_d} \qquad (Eq.\ 4.5)$$

where B and F is the density of bound and free ligands in the cell-SLB contact, respectively, $N_t f/S_{cell}$ is the density of mobile receptors on the cell and p is the ratio between the contact area, S_b, and the total cell surface area, S_{cell}:

$$p = \frac{S_b}{S_{cell}} \qquad (Eq.\ 4.6)$$

The total cell surface area can be calculated by measuring its cross-sectional area, *A*, in the microscope and thereafter using the following relationship:

$$S_{cell} = 4 \cdot A \cdot 1.8 \qquad (Eq.\ 4.7)$$

where where the factor 1.8 accounts for the roughness of the cell membrane (92).

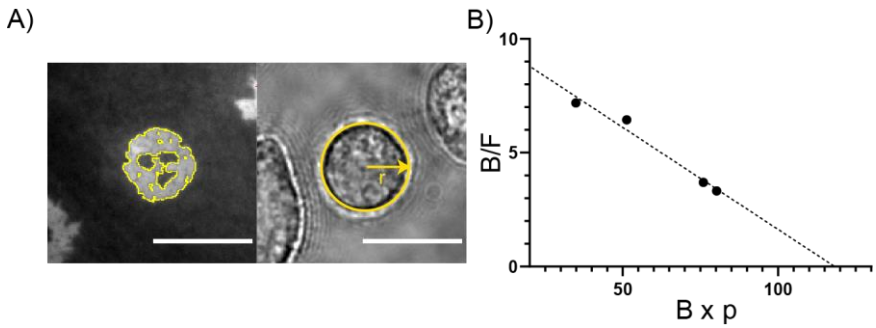

Figure 4.1: (A) (left) A representative image of a cell-SLB contact showing accumulation of fluorescently labelled ligands and (right) a brightfield image of the cell forming the contact. **(B)** A Zhu-Golan plot from which the 2D K_d of the interaction is derived from the negative reciprocal of the slope and the mobile receptor density is derived from the curve's intersect with the x-axis. Reproduced with permission from (89).

In this thesis, the Zhu-Golan method was used by preparing multiple SLBs with His-tagged ligands at different densities, going from low to high. Jurkat T cells, which expressed the corresponding receptors, were then deposited onto the SLBs after which protein binding would occur. The experiment was imaged using TIRF microscopy and since the proteins were fluorescently labelled, protein binding in the membrane interface was visualized as fluorescent accumulation underneath the cell. This region will henceforth be referred to as the contact area. The mean intensity, $I_{cell\text{-}SLB}$ in the contact area is proportional to $B+F$, which can be obtained by outlining the contact area in an image analysis software and measuring the mean intensity (all image analysis in this work was done using Fiji ImageJ). Converting $I_{\text{cell-SLB}}$ into $B+F$ can be done by relating this intensity to the intensity from one ligand, $I_{protein}$, measured by single molecule imaging (18, 88). The density of free ligands outside the cell contact, F^*, is in turn proportional to the measured intensity in the area surrounding the contact area, I_{SLB}. However, the density of free ligands within the contact area, F, is generally lower than this value due to steric exclusion (87, 88). The extent of this exclusion can be estimated by mixing in fluorescently labelled non-binding proteins of similar size to the protein of interest and quantify the difference in signal from this protein inside and outside the contact.

Since each cell has a different receptor density this means that also B and p will vary among the cells. Thus, average B/F and $B \cdot p$ values was calculated for many cell-SLB contacts for each SLB containing a certain ligand density, providing one data point on the Zhu-Golan plot. Repeating this for SLBs with different ligand densities resulting in multiple points which could be fitted to Eq. 4.5 from which the negative reciprocal of the slope gave the 2D K_d of the interaction and the intersect with the x-axis the average density of mobile receptors per cell (Figure 4.1B).

At high ligand densities the cell can start to spread and form abnormally large contacts through lamellipodia structures (88). In such contacts, the B/F value is generally higher compared to non-lamellipodia forming contacts (88). By including contacts with lamellipodia structures into the Zhu-Golan analysis, the obtained curves will give erroneous values and contacts with lamellipodia structures were therefore avoided from all Zhu-Golan analysis in this thesis.

4.2.3 Measuring single-cell binding affinities

The Zhu-Golan method outlined in the previous section requires measuring B/F and $B \cdot p$ values for a large number of contacts to form a reliable cell population average. This process often requires a substantial amount of time to gather the data, as well as to analyze it. In addition, the resulting 2D K_d and the receptor density derived from the Zhu-Golan analysis is therefore also a population average. However, the 2D K_d could potentially vary from one cell to another due to environmental factors, different stages in the cell cycle and due to genetic variations. To be able to capture cell variations in 2D K_d and to reduce the time spent on the experiments, a modification to the Zhu-Golan analysis was developed in Paper II in order to be able to measure affinities on single cells.

To measure single-cell binding affinities, an SLB functionalized with a high ligand density is used. Receptor-expressing cells are then deposited onto the SLB whereupon contact areas are formed as a consequence of protein binding, as in the case of the classical Zhu-Golan analysis (Figure 4.2). The system is allowed to incubate and reach equilibrium before the necessary imaging of the contact areas and the cell itself is performed. Imidazole is then added to the sample competing with the His-tagged proteins for binding to DGS-NTA(Ni). As such, the protein density decreases as long as imidazole is present in the sample well. Once the protein density has dropped by approximately half the sample is washed thoroughly with excess filtered buffer to remove the presence of imidazole in the sample. The system is then allowed to reach equilibrium once again before imaging all the contact areas and cells. In such, imidazole is used to bring the protein density through the same density increments as when the classical Zhu-Golan experiments are done (91). This is typically repeated a few times to give 3-4 separate data points in a Zhu-Golan plot, where each data point now is from a single cell-SLB contact.

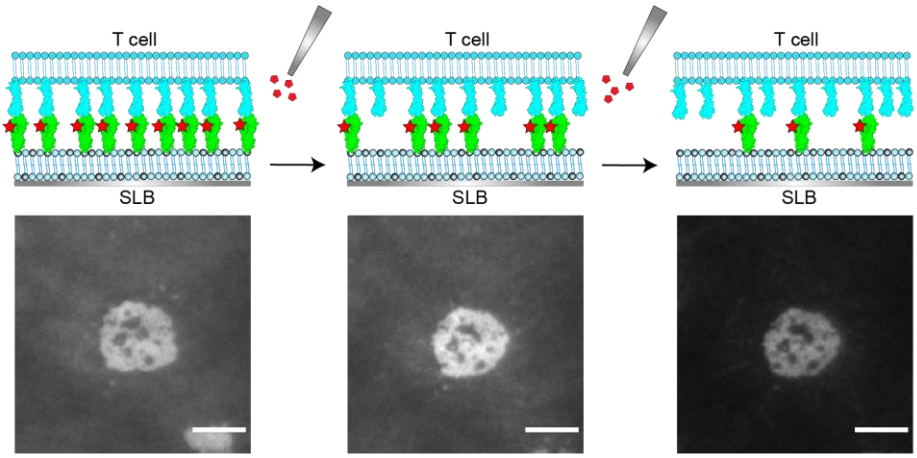

Figure 4.2: A schematic illustration of the protocol for performing single-cell binding affinity measurements. Individual cell-SLB contacts are imaged at subsequent different ligand densities which are achieved through titration with imidazole. Images are captured 40 minutes after ligand titration and the scale bars are 5 µm.

4.2.4 Measuring 2D lifetimes using fluorescence-based binding assays

Whereas the Zhu-Golan method has been extensively used to measure 2D K_d values it does not provide information on the lifetime of the interaction. Here other fluorescence-based approaches can be used. One example of a fluorescence-based approach to measure the lifetime of an interaction is to utilize FRAP. In this technique, fluorescently labelled ligands are incorporated into a SLB and are allowed to interact with a cell expressing the corresponding receptors, as in the Zhu-Golan method. By bleaching the ligands in the contact and monitor the recovery, the lifetime of the interaction can be estimated (93, 94). This technique has been used to investigate the binding 2D lifetime between CD2 and CD58 where it was found to be 14 s, 100 times higher compared to the 3D counterpart (59), further illustrating the differences in protein binding in 2D and 3D. However, there is a limit of 5-10 s for how short the lifetimes can be accurately measured if the bleached area is 5-10 µm wide. For any shorter lifetimes, the diffusion will dominate the recovery process (88, 95). An alternative to measuring the lifetime by monitoring the mobility of a larger protein population is to instead use single-molecule imaging. Here, single fluorescently labelled proteins are located with nanometer spatial resolution and the movements are tracked (96). Binding events between receptors and ligands can be detected from a change in diffusion (97), reduced motion blur in image acquisitions with high exposure time (98) or by using Förster Resonance Energy Transfer (FRET). In FRET the receptor and ligand are tagged with different fluorophores and when the ligand and receptor are bound, a FRET signal is generated through a non-radiative energy transfer (99, 100). Huppa et al. used this technique to study binding between the 2B4 and 5c.c7 TCR system to binding to different pMHC molecules

(IE^k/MCC, IE^k/T102S and IE^k/K99R) revealing k_{off} values 3-12 times higher than their 3D counterparts (101). The difference was less distinguishable when the cells were treated with actin-depolymerizing drugs which suggests that the cytoskeleton could exert a force on the TCR-pMHC bond which decreases the lifetime, a characteristic slip bond behaviour (101). O'Donoghue et al. detected binding events of single AND TCRs and 5c.c7 TCRs binding to IE^k and MCC through a reduced motion blur during image acquisition (98). In contrast to Huppa et al. the measured k_{off} values measured in 2D was similar to the 3D counterpart regardless of whether the cells were treated with actin-depolymerizing drugs (98). While there are discrepancies in the single-molecule imaging studies, the technique has the advantage of being able to monitor rare binding events which could have been obscured if population averages were measured instead. By examining the lifetime distribution of binding events between AND TCR and IE^k/MCC it was found that the T cell response was largely governed by disproportionally strong and long-lived binding events that were orders of magnitudes longer than the average binding event (102).

4.3 2D vs 3D binding theory

As it has been described above, measuring binding kinetics in two-dimensions is difficult. The measured values of affinities and kinetic rates have been shown to vary depending on whether the employed method is fluorescence-based or mechanical-based. Meanwhile measuring the same kinetic parameters in 3D have been easier through SPR, but less representative of the biological environment. An alternative approach has been to establish a relationship between the binding equilibrium constants in 3D and 2D. One issue with directly comparing these two entities is the difference in units. Per definition, the equilibrium constant in 2D has units of molecules per area while the 3D counterpart is in molecules per volume. The ratio between the 2D and the 3D K_d is a characteristic length, h, (103):

$$K_d^{2D} = h \cdot K_d^{3D} \qquad (Eq.\ 4.8)$$

which corresponds to the maximum distance between a ligand and a receptor before they can interact. Measuring h has been done using fluorescence-based and micropipette-based methods. However, the fluorescence-based methods yield a characteristic length on the nanometer-scale while the micropipette-based methods yield a length on the micrometer-scale (104). The former is more intuitively reasonable based on the extent of typical interaction potentials between molecules, however, the micropipette-based methods are performed on initial bond where h might have a different meaning compared to on already established contacts with multiple bonds (104).

Various simulations have been performed to understand the differences between 2D and 3D binding better. These studies reveal that the 2D K_d, k_{off} and k_{on} are influenced by factors such as membrane roughness (105–107) and protein flexibility (108). Monte Carlo simulations show that tall rod-like ligands with high flexibility can adopt a lower effective height and occupy a large surface area which counteracts aggregation of other ligands due to repulsion from the rotation around its anchor point (18). Furthermore, the flexibility of a tall rod-like ligand can affect the imposed entropic penalty during binding which can effectively lower the binding affinity (108). Protein binding between membrane-bound species decreases membrane fluctuations, which in turn facilitates more protein binding due to less deviation from the optimal binding distance (106). In molecular dynamics (MD) simulations the optimal membrane separation was found equal the length of the receptor-ligand pair (106). Increasing the membrane roughness from the optimal distance resulted in a higher 2D K_d (105, 106). These studies reveal that membrane fluctuations hinder protein association but also suggest that adding more degrees of freedom, by increasing membrane fluctuations, increases protein dissociation.

5. T cell signaling and model membrane surfaces

5.1 TCR signaling

While the immune response is complex and specific to the pathogen invading the host, the initiating step is commonly agreed upon to be the interaction between TCR and pMHC. As previously mentioned, the TCR is a heterodimer and is most commonly composed of an α-chain and a β-chain. The receptor itself does not have any signal-transducing activity due to a lack of immunoreceptor tyrosine-based activation motifs (ITAM). However, the TCR non-covalently associates with a group of CD3 subunits which includes: CD3ε, CD3γ, CD3δ and CD3ζ. The CD3ε, CD3γ and CD3δ each carry one ITAM while CD3ζ carry three ITAMs. The TCR and CD3 often associate with the stoichiometry of TCRαβ-CD3εγ-CD3εδ-CD3ζζ which results in 10 ITAMs per TCR complex (109, 110). To initiate TCR signaling, the ITAMs of the TCR-complex needs to be phosphorylated by Lck. This process is amplified by the coreceptors CD4 or CD8 (depending on whether the T cell is either a $CD4^+$ helper cell or a $CD8^+$ cytotoxic cell) expressed by the T cell (111). The intracellular parts of the coreceptors bind to Lck which phosphorylates the ITAMs of the CD3 subunits once recruited to the contact area. The phosphorylation of the TCR-complex further proceeds with the recruitment of the protein tyrosine kinase ZAP70 which is itself phosphorylated and activated by Lck. The ZAP70 acts as a scaffold for the transmembrane adaptor linker for activation of T cells (LAT). The phosphorylation of LAT by ZAP70 leads to further recruitment of other intracellular adaptor molecules to form a large complex that leads to calcium release, cytoskeleton remodelling and the activation of transcription factors such as nuclear factor of activated T cells (NFAT). These transcription factors alters the proliferation, cytokine production and the effector functions of the T cell (109, 112).

5.2 Initiating TCR phosphorylation

While large portions of the intracellular process of T cell activation is mapped out, the initiating molecular mechanism is not clear. The unknown molecular mechanism has to be able to initiate a sufficiently strong signal when the T cell is presented with

an agonist peptide and remain passive when presented with an endogenous peptide. In addition, endogenous peptides are more abundant on the surface of an APC compared to agonist peptides. T cells have been reported to undergo activation when as few as 1-10 pMHCs are expressed on the T cells (113–115). As a consequence, the initiating mechanism for T cell activation has to both have high selectivity and high sensitivity.

Given that the TCR-pMHC interaction is widely viewed as the initial interaction for T cell activation, considerable work has been invested into characterizing the binding kinetics of this interaction and how this relates to T cell activation. One of the early models for T cell activation, referred to as the kinetic proofreading model, postulates that the TCR-pMHC interaction has to be maintained for a long enough time for the intracellular signaling process to be completed. The kinetic proofreading model therefore predicts that there is a relationship between the dissociation rate in the TCR-pMHC interaction, and the activation potency of the pMHC (82, 110). Matsui et al. observed that pMHCs that elicit weak T cell responses are accompanied by high k_{off} values (0.09 s^{-1}) compared to pMHCs that elicit stronger T cell responses (0.3-0.06 s^{-1}) (116). Such observations indicate that the molecular mechanism, behind the T cell antigen recognition process, revolves around how fast TCR and pMHC dissociates after binding. Further support came from observations that antagonistic pMHCs complexes could have 100-fold higher k_{off} values together with a lower affinity (500-1500 µM) compared to the examined agonistic pMHCs (117). Such TCR-pMHC interactions are too short-lived before the necessary intracellular events can lead to a proper T cell response. However, these measurements were done using SPR and does not necessarily reflect the binding kinetics when both receptors and ligands are anchored to the membrane. In addition, a few outliers have been reported where ligands act as weak agonists despite having a slow dissociation rate (63). Another model, which takes advantage of the seemingly intrinsic weak interaction between TCR and pMHC, is the serial triggering model. The model postulates that a single pMHC can initiate T cell signaling by interacting with multiple TCRs. A few results provide an indication of this. Tolentino et al. reported a 100 times slower dissociation rate (0.074 s^{-1}) compared to the 3D counterpart. A possible explanation for this observation is that CD2 and CD58 rebind multiple times before diffusing far enough away where the two species cannot interact (59). One of the predictions from the serial triggering model is that there should be an optimal dwell time in the TCR and pMHC interaction which allows for effective T cell activation (63, 118, 119). While this contradicts the prediction by the kinetic proofreading model, using a micropipette assay Huang et al. found that the measured 2D k_{off} for the investigated pMHCs were found to be 8300-fold faster than the 3D counterpart. Such fast dissociation could suggest that serial engagement could be a part of the initiating mechanism (73). However, while studies using pMHC tetramers have indicated an optimal dwell time between TCR and pMHC for an effective T cell activation (120), there has been a lack of supporting evidence using monomeric TCR (63, 119).

In addition, other models have been developed to explain the high sensitivity to agonistic pMHCs (113). An example of such a model is the conformational change model which postulates that an agonist pMHC binding to TCR induces conformational change to the TCR/CD3 complex in such a way that ITAMs become more accessible for phosphorylation (121, 122). Another model is the pseudodimer model which takes advantage of the fact that the number of self-peptides outnumber the amount of presented non-self peptides on the surface of APCs. A dimer can form between two TCRs binding either an agonist pMHC and a low-affinity self-peptide MHC (111, 121). This dimerization is enhanced by coreceptors which is associated with one TCR while simultaneously engaging the agonist pMHC. The close proximity to coreceptors then also facilitates Lck-mediated phosphorylation (123). One model that during recent years have gained in popularity is the kinetic segregation model, which is described in short below.

5.2.1 The kinetic segregation model

TCR phosphorylation is carried out by the kinase Lck. Conversely, dephosphorylation of the TCR is carried out by the phosphatase CD45. In a resting T cell, the latter of these two processes dominates leaving unphosphorylated TCRs. However, the kinetic segregation model postulates that size-based segregation of CD45 in the cellular contacts created by TCR-pMHC binding shifts this balance towards Lck phosphorylation (Figure 5.1) (69, 119). The size of the narrow membrane gap is set by the dimensions of the TCR-pMHC complex, which is approximately 13 nm in height (13, 124). In contrast, CD45 has a height between 20-40 nm depending on its isoform (18). Therefore, when the T cell makes a contact with an APC by forming contacts comprised of TCR-pMHC, the membrane gap is too small to accommodate the CD45. As such, the CD45 is segregated away from the cell contact region leaving the TCR open to be phosphorylated by Lck. The amount of time the TCR is phosphorylated depends on the interaction time between TCR and pMHC. When the TCR dissociates from the pMHC it swiftly departs the close-contact region by diffusion and is dephosphorylated by CD45.

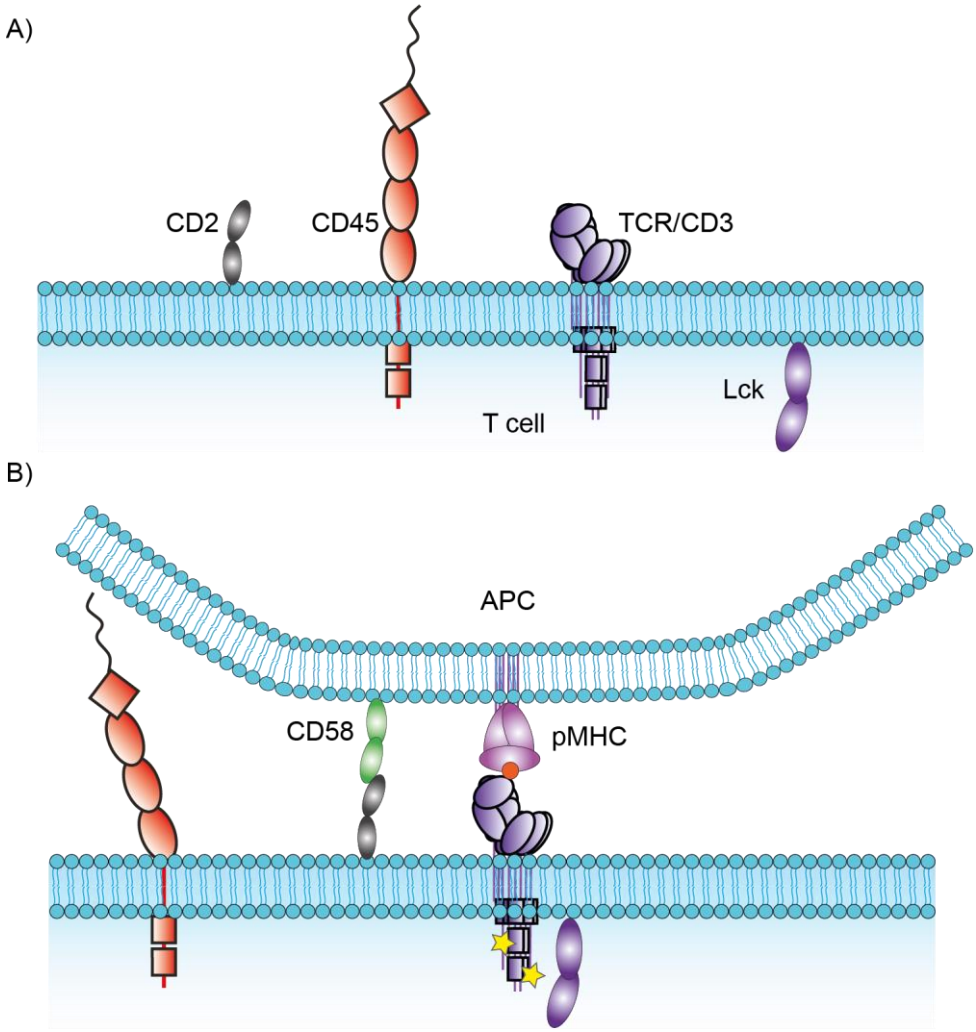

Figure 5.1: Illustration of the kinetic segregation model.
(A) In a resting T cell, the various membrane proteins are randomly distributed on the surface of the T cell. **(B)** The approach of an APC results in the formation of a contact region through TCR/pMHC and CD2/CD58 binding. Establishing a contact region results in a membrane gap which excludes the taller CD45 molecules. The exclusion shifts the ratio between the intracellular Lck and CD45 inside the contact in favour of the former, resulting in TCR phosphorylation.

There have been convincing arguments to support the concepts in the kinetics segregation model. Support for size-based segregation of CD45 can be found in studies using shortened forms of CD45 which observed less CD45 exclusion (125, 126). Similar findings have been found where lower amounts of CD45 exclusion is observed the dimensions of the TCR-pMHC binding complex has been increased (124). T cells that lack CD45 or express a truncated CD45 does not undergo TCR

triggering (127). However, CD45 is also known to activate Lck by dephosphorylating its C-terminal inhibitory tyrosine. The role of CD45 in initiating TCR triggering is therefore more multifaceted. Other studies have examined the role of other phosphatases, such as CD148, that do not activate Lck and found a higher propensity for TCR triggering when CD148 exclusion occurred (126, 128). Furthermore, CD45 exclusion has also been demonstrated using CD45 functionalized GUVs interacting with SLBs (129) which suggests that the size-based protein exclusion in the KS-model is a passive effect and can occur without the involvement of the cytoskeleton in the initial stages. In addition, T cells are not readily activated when using soluble antibodies. This could be explained by the lack of an opposing membrane attachment which would form a membrane gap to drive the size-based segregation of proteins. Instead, when using immobilized anti-TCR it has been observed that CD45 is excluded from triggering TCRs (130). However, a few studies have demonstrated that sufficiently high affinity ligands can initiate TCR triggering in the absence of CD45 exclusion (131, 132). While weak binding ligands are more potent to activate T cells when there is higher CD45 exclusion, elongated high affinity ligands have been demonstrated to also be able to induce TCR triggering even in the absence of CD45 exclusion (131, 133). However, a compelling observation that kinetic segregation is important in initiating T cell activation is that it agrees with observations of ligand independent triggering, an effect that cannot be explained with most other models of T-cell activation (134). In this, TCR triggering can occur without the TCR engaging pMHC or any other binding molecule. To test this, close-contact regions of similar intermembrane distance as set *in vivo* by TCR-pMHC can be made in vitro using other binding molecules, e.g. the rCD2-rCD48 pair (88). TCRs within such contacts will according to the kinetics segregation model stay phosphorylated until they by diffusion leaves the contacts. If the contacts are sufficiently large this can lead to downstream signaling, even without any TCR engagement by pMHC.

5.2.2 Ligand-independent triggering

As discussed in the previous section, the kinetic segregation model allows for ligand-independent triggering in the absence of a TCR ligand under certain circumstances. Such observations have recently been reported in several studies (20, 134–136). Chang et al. created large close-contact regions by binding rCD48 expressing T cells to rCD2-functionalized SLBs (20). T cell activation was confirmed by calcium release and found that even in the absence of pMHC ~60% of the cells signalled (20). Fernandes et al. related this to the likelihood of a TCR staying inside the contact region as a function of the contact size (134). It was shown that calcium release by ligand independent triggering indeed depended on the size of the close contacts and that to achieve ligand-discrimination, it was important that contacts that are not larger than ~200 nm in radius. This is similar to the radius of microvilli protrusions on T cells argued to be the initial points of TCR-pMHC

interaction *in vivo* (137, 138). If the close-contact regions have larger radius the cell could trigger regardless of peptide potency due to the likelihood of the TCR remaining in a phosphatase-depleted region being significant regardless of TCR binding pMHC.

Ligand-functionalized SLBs are commonly used to study ligand discrimination and T cell activation by detection of calcium release (115, 139–141). However, various studies have demonstrated that T cells are able to undergo activation even without any specific TCR interaction, including SLBs containing non-TCR ligands (142, 143) as well as glass surfaces coated with nonspecific IgG (20) and PLL (136). Thus, it is important to characterize and understand the conditions that facilitate ligand independent triggering in order to distinguish it from ligand-dependent triggering events. In many of these studies SLBs are often used to replace the membrane of an APC. Incorporating nickel-chelating lipids such as DGS-NTA (Ni) is commonly used to functionalize the SLB with Histidine-tagged proteins. However, as demonstrated by Ponjavic et al. the presence of DGS-NTA(Ni), can by itself induce LIT in T cells (143). Whether this effect also applies when having a ligand-functionalised SLB, if it is a consequence of kinetic segregation, or another molecular mechanism, and how to minimize this effect was investigated in Paper I.

5.3 Triggering on ligand-free SLBs

To detect T cell activation via calcium release, as Jurkat T cells are interacting with SLBs containing different densities of DGS-NTA(Ni), the cells were loaded with the fluorescent calcium-sensitive dye Fluo4-AM. Upon T cell activation, the cell releases calcium ions from internal depots into the cytoplasm. The Fluo4-AM binds to the calcium ions which increases its fluorescence significantly. Non-triggered cells remain on the surface with a much relative lower fluorescent intensity due to no significant increase in calcium concentration in the cytoplasm. The characteristics of a triggered cell and a non-triggered cell that are used to detect the cells are described in the next section.

5.3.1 Detecting calcium release

A custom-written MATLAB-script was used to detect and quantify the fraction of signaling cells. The input is a video-file showing the cells at different times after landing on the surface (Figure 5.2A). After some time, if the surface interaction results in T cell signaling, the cell will undergo calcium release which is detected as a rise in intensity due to the loading of Fluo4-AM. A characteristic intensity graph of a triggering cell is shown in Figure 5.2B. The cells emit a weak fluorescence even before calcium release and there is thus an intensity increase giving a “baseline”

signal when the lands. The intensity then rises sharply when calcium is released before calcium then starts to be transported away from the cytosol, resulting in a peak intensity and then subsiding to a lower intensity as cell “recovers”. In contrast, the intensity profile of a non-triggering cell shows an intensity rise upon cell landing but remains relatively unchanged throughout the measurement (Figure 5.2C).

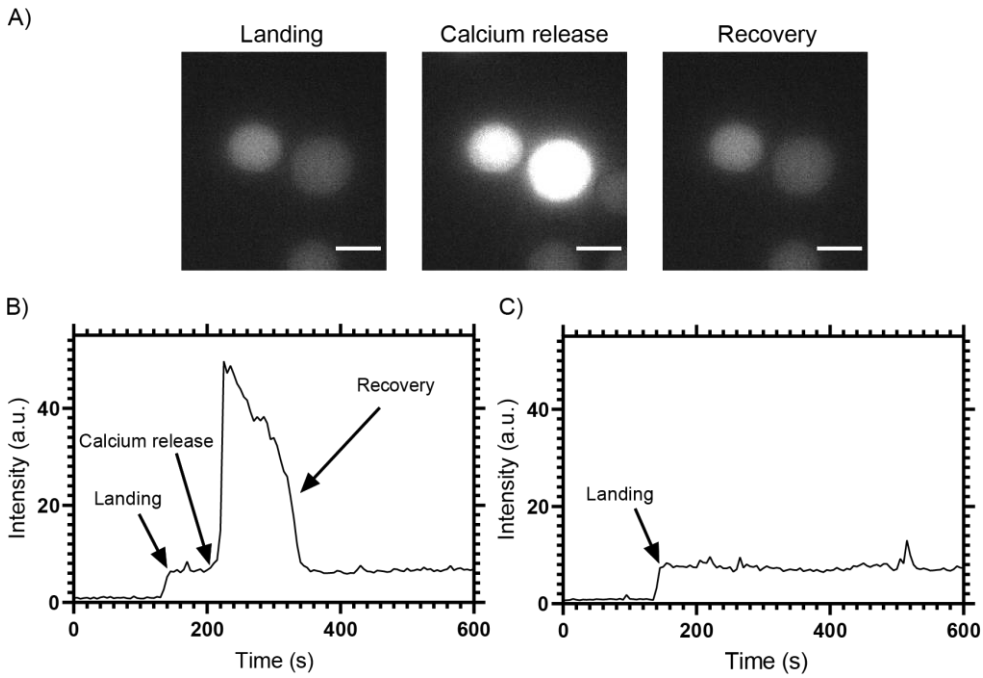

Figure 5.2: (A) Representative fluorescence microscopy images of a signaling cell during the different stages of the calcium release. **(B)** An intensity profile characteristic of a signaling cell at different times. **(C)** An intensity profile characteristic of a non-signaling cell. Scale bar is 10 µm.

The MATLAB script detects every cell in each frame of the video file and saves the cell location. The mean intensity of the cell-occupied location is measured throughout the video file and produces an intensity profile as exemplified in Figure 5.2C and Figure 5.2D. A cell is deemed triggered if the peak intensity is 2.5 times larger than the ”baseline” intensity. It is important to ensure that the detected calcium release occurs as a consequence of surface interactions. Therefore, any cell where the intensity peak comes within the first five frames after landing is discarded from the analysis. Every intensity profile is saved which can be reviewed and can be corrected for by the user. When the review process is completed, the program outputs the signaling fraction.

5.3.2 Calcium signaling due to DGS-NTA(Ni)

Cell adhesion was investigated on SLBs containing 1, 2, 5 and 10 wt% DGS-NTA(Ni). Jurkat T cells were deposited onto the SLBs and after 15 minutes bright field images were taken of the cells at various positions on the SLB (Figure 5.3). Afterwards, the samples were washed with filtered HBS buffer and bright field images were anew taken at the same positions as before the washing step. No cell adhesion was observed for a pure POPC SLB but 50 % of the cells adhered to the SLBs containing 1 wt% DGS-NTA(Ni). At 2 wt% DGS-NTA(Ni) and above, almost all cells adhered to the SLB. When treating the SLBs with a solution of EDTA that strips away the nickel ions from the DGS-NTA(Ni), the cells again did not adhere to the SLBs, indicating that the divalent cations are key to the unspecific cell interaction.

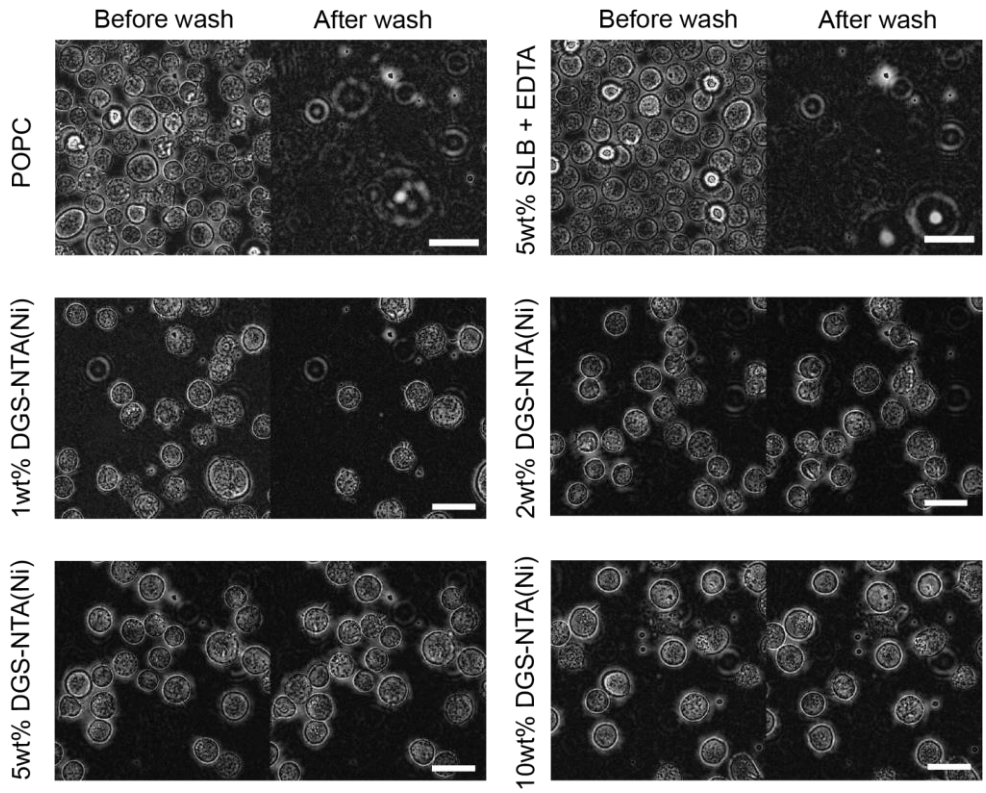

Figure 5.3: The presence of DGS-NTA(Ni) in the SLB induces cell adhesion.
A collage of bright field images of cells resting on SLBs with DGS-NTA(Ni). For densities between 2 and 10 wt%, virtually all cells adhered to the SLB. Images were taken before (left) and after (right) washing. The cells were deposited onto the SLBs and left to incubate for 15 minutes, the same measurement time used in the triggering experiments, before the surfaces were washed with filtered HBS buffer. For comparison, no cell adhesion was observed on a pure POPC SLB or on a SLB treated with EDTA. The scale bars are 10 µm. Reproduced with permission from (89).

Calcium signaling was then investigated on 2, 5 and 10 wt% DGS-NTA(Ni) SLBs since the level of cell adhesion was high on these bilayers. Cells were loaded with Fluo4-AM and deposited onto the SLBs. After addition, a fluorescence image acquisition with a 5 second interval between frames were started. The image acquisition was analyzed as described in section 5.3.1 to obtain a mean signaling fraction of cells for the SLBs containing different amounts of DGS-NTA(Ni). All SLBs could induce calcium signaling to some extent but the signaling fraction was found to increase with the concentration of DGS-NTA(Ni): 24% at 2 wt%, 41% at 5 wt% and 60% at 10 wt% (Figure 5.4).

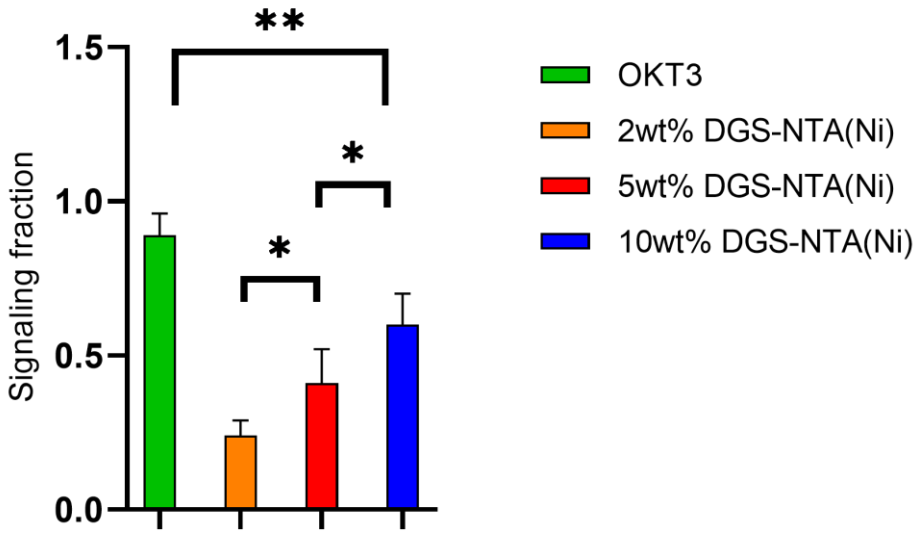

Figure 5.4: The signaling fraction of Fluo4-AM loaded Jurkat T cells on anti-CD3 antibody OKT3 and SLBs with a DGS-NTA(Ni) concentration ranging from 2 wt% to 10 wt%. The cells were allowed to interact with the SLBs for 15 minutes with images taken every 5 seconds. The signaling fraction was the highest on OKT3, measured to 89 ± 7 %. Thereafter the average signaling fraction was shown to increase from 24 ± 5 % on 2 wt%, 41 ± 11 % on 5 wt% to 60 ± 10 % on 10 wt%. The values are mean ± SD from 5-8 experiments and a two-sample t-test in MATLAB was used for statistical analysis with: * <0.05, ** <0.01, *** <0.001. Adapted with permission from (89).

As a positive control, experiments were also performed on anti-CD3 (OKT3) - covered glass slides, yielding a signaling fraction of 89% (Figure 5.4), which is similar to previous reported values (136, 143, 144). The signaling fraction for SLB containing DGS-NTA(Ni) was always lower than the signaling fraction on OKT3-covered surfaces, even though the density of DGS-NTA(Ni) would be much higher than the density of OKT3 on the surface. Thus, although still significant, the triggering mechanism by DGS-NTA(Ni) is less efficient at initiating calcium signaling than the antibody. Whether this was influenced by having ligands on the SLB is discussed in section 5.4.

5.4 Including ligands in the SLB does not significantly influence signaling by DGS-NTA(Ni)

As ligand-free SLBs containing DGS-NTA(Ni) was shown to induce cell adhesion and calcium signaling on Jurkat T cells, the next step was to investigate whether this was also the case for the biologically more relevant situation when having ligands in the SLB. SLBs containing either 5 wt% or 10 wt% DGS-NTA(Ni) were functionalized with His-tagged rCD2 which binds a high affinity mutant of rCD48 ($rCD48_{T92A}$) expressed on the Jurkat T cells (Figure 5.5A). This binding pair have a similar height as that of TCR-pMHC, but with $rCD48_{T92A}$ being a non-signaling molecule on the cells. Protein densities of rCD2 up to 2000 molecules/μm^2 were further used, but the signaling fraction remained independent of rCD2 density and was within the error of the measured signaling fraction for the ligand-free SLBs (Figure 5.5B). This supports the notion that interactions with DGS-NTA(Ni) dominates the triggering mechanism in studies.

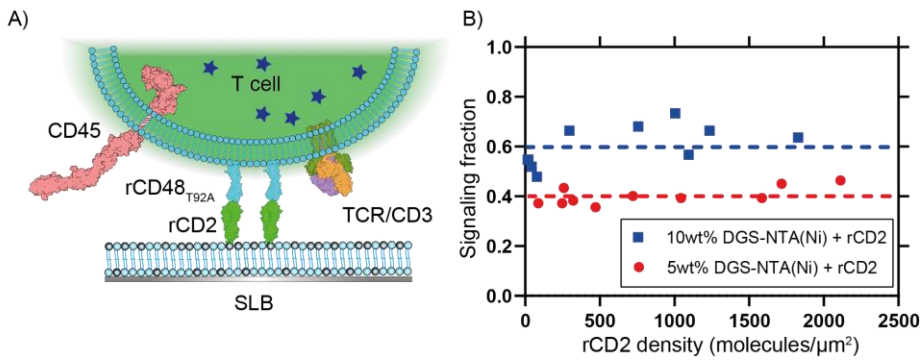

Figure 5.5: Calcium signaling is dominated by DGS-NTA(Ni) interactions.
(A) Schematic illustration showing Jurkat T cells expressing a non-signaling $rCD48_{T92A}$ being deposited onto a SLB with either 5 wt% or 10 wt% DGS-NTA(Ni) which is functionalized with rCD2. **(B)** The signaling fraction on SLBs containing either 5 wt% (red), or 10 wt% (blue) DGS-NTA(Ni), with various rCD2 densities. Each data point represents one experiment where 150 cells were analyzed. The dashed lines represent the measured signaling fraction on ligand-free SLBs. Adapted with permission from (89).

5.5 Blocking the DGS-NTA(Ni) interactions with BSA

To block the nickel-chelating lipids, a 5% bovine serum albumin (BSA) solution was used. This was found to effectively prevent cell adhesion and essentially no cells remained attached after washing compared to without blocking when all cells were attached (Figure 5.6).

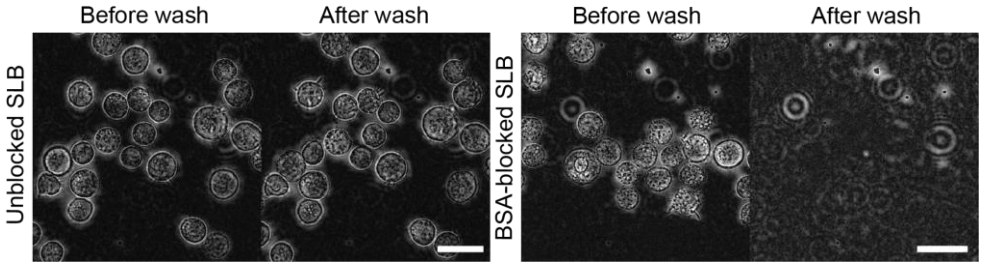

Figure 5.6: Unspecific cell adhesion on SLBs, with 5 wt% DGS-NTA(Ni), is prevented when blocking with BSA. A collage of bright field images of cells resting on SLBs with 5 wt% DGS-NTA(Ni) either without (left) or with (right) BSA blocking. The scale bars are 10 µm. The cells were deposited onto the SLBs and left to incubate for 15 minutes, the same measurement time used in the triggering experiments, before the surfaces were washed with filtered HBS buffer. Reproduced with permission from (89).

Having found a way to reduce unspecific cell interactions, the cell triggering experiments on protein-functionalized SLBs were revisited, with the addition of BSA-blocking (Figure 5.7A). Notably, the signaling fraction dropped to 11 % regardless of rCD2 density and was furthermore not dependent on DGS-NTA(Ni) concentration, the latter indicating a high effectiveness at blocking interactions with DGS-NTA(Ni) (Figure 5.7B).

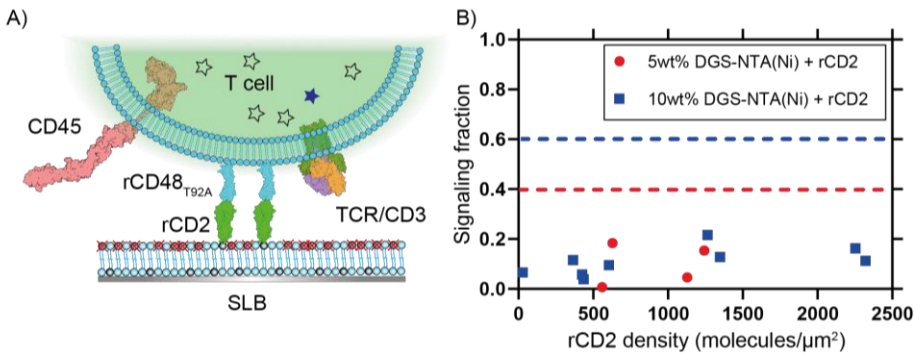

Figure 5.7: BSA blocking reduces the signaling fraction significantly.
(A) Schematic illustration showing Jurkat T cells expressing a non-signaling $rCD48_{T92A}$ being deposited onto a BSA-blocked (red crosses) SLB with either 5 wt% or 10 wt% DGS-NTA(Ni) which is functionalized with rCD2. **(B)** The signaling fraction on BSA-blocked SLBs containing either 5 wt% (red), or 10 wt% (blue) DGS-NTA(Ni), at various rCD2 densities. Each data point represents one experiment where 150 cells were analyzed. The dashed lines represents the measured signaling fraction on non-blocked, ligand-free SLBs. Adapted with permission from (89).

5.6 DGS-NTA(Ni) interacts with TCR but does not influence CD45 exclusion

The exclusion of CD45 is a key component in the kinetic segregation model and to investigate whether an increased CD45 exclusion is the main driver behind TCR triggering by DGS-NTA, the Jurkat cells were marked with Alexa Fluor 647-labelled antibodies against human CD45 (clone HI30). The cells were then deposited onto low-triggering (BSA-blocked) surfaces and higher-triggering (non-blocked) surfaces after which the CD45 distribution in the cell contacts were imaged (Figure 5.8A). To evaluate the level of CD45 exclusion, the intensity from the labelled antibodies inside the contact was compared with the intensity outside the contact (Figure 5.8B). The analysis revealed that there was 79 % less CD45 present in the contact for both blocked and non-blocked surfaces. Thus, the increase in cell signaling caused by DGS-NTA(Ni) was not due to increasing CD45 exclusion.

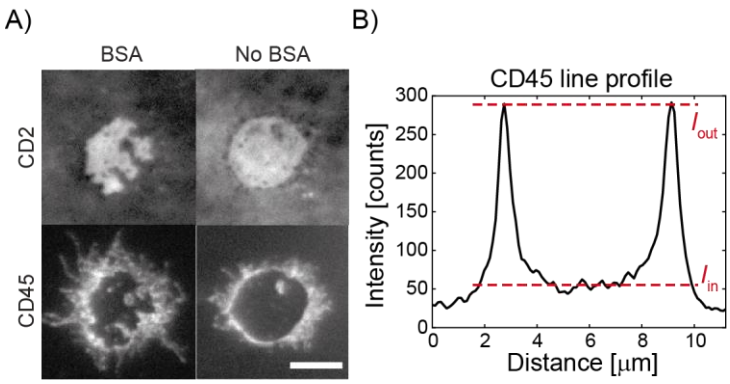

Figure 5.8: Blocking does not influence CD45 exclusion.
(A) Jurkat T cells labelled with fluorescent anti-CD45 antibodies adhered via rCD2/rCD48$_{T92A}$ binding on (left) a BSA-blocked SLB and (right) a non-blocked SLB. **(B)** A representative line profile through a cell-SLB contact from which the CD45 intensity inside, I_{in}, and outside, I_{out}, is obtained, resulting in a CD45 exclusion in the contact of 79% regardless of whether BSA blocking was used or not. Reproduced with permission from (89).

To investigate whether the calcium release was indeed TCR dependent, measurements on unblocked DGS-NTA(Ni) SLBs were performed with TCR-deficient J.RT3-T3.5 cells. These measurements gave low cell signaling fractions (<10 %) with both blocked and unblocked SLBs, indicating that the calcium release required TCR triggering. It is therefore possible that DGS-NTA(Ni) acts as a weak ligand towards TCR, which additionally could reduce the TCR's effective mobility and increase its local density in the contact regions. The former will keep the TCR in the close contact regions for a longer time, increasing the likelihood for signaling, as argued by Chen et al. (144). It is also possible that interactions with DGS-NTA(Ni) increases the local density of phosphorylated TCRs to exceed a threshold

required for calcium signaling. As such, the higher the TCR density on the cell, the higher the propensity to undergo calcium signaling (134). Such factors could also to some extent explain the discrepancy in our observed (low) signaling fraction compared to other studies where rCD2-rCD48$_{T92A}$ binding have resulted in significantly higher levels of ligand independent triggering (20).

5.7 Summary

The results in Paper I demonstrate that the choice of lipid composition in the SLB affects the degree of cell adhesion, which in turn also influences the level of triggering. Specifically, in the commonly used SLB systems which uses DGS-NTA(Ni) as a linkage system to attach His-tagged proteins, the signaling fractions were found to increase with the concentration of DGS-NTA(Ni) in the bilayer. This was also the case when having the His-tagged rCD2 protein in the SLB at densities up to 2000 molecules/μm^2, which did not influence the measured signaling fractions. However, using a 5 % BSA solution as a blocking agent did have a significant effect and prevented cell adhesion on ligand-free SLBs and significantly lowered the signaling fraction to a base level regardless of DGS-NTA(Ni) concentration in the SLB.

How DGS-NTA(Ni) causes T cell signaling is still speculative but experiments with TCR-deficient J.RT3-T3.5 cells indicate that the calcium signaling occurs via TCR triggering. No increase in CD45 exclusion was found due to DGS-NTA(Ni)-cell interactions, indicating that an increased ligand independent triggering caused by CD45 exclusion was not dominating this effect. It is instead possible that DGS-NTA(Ni) is acting as a weak ligand towards TCR, causing TCR to locally accumulate in the contact region where CD45 is excluded. Due to this effect, it is important to block these interactions whenever TCR triggering is investigated as a function of receptor-ligand interactions. For this purpose BSA (which also contains several histidines) can be used, which was found to prevent cell adhesion and significantly lowered the signaling fraction due to DGS-NTA(Ni) interaction.

6. The height of ligand-receptor pairs influences binding and organization in cell contacts

6.1 Introduction

The 2D binding affinity, and subsequently binding kinetics, of TCR has been measured in a large number of studies to shed light on the mechanism behind antigen recognition. As mentioned in section 4.2, fluorescence-based and micropipette-based assays have been used to measure these values for TCR-pMHC binding pairs but often these studies only included the TCR-pMHC pair alone, neglecting the influence of auxiliary molecules such as adhesion molecules, coreceptors and costimulatory molecules. The aspect of size in adhesion molecules is thought to be important as adhesion molecule pairs of similar height as TCR-pMHC, such as CD2-CD58, are thought to facilitate TCR-pMHC interactions (as described in section 1.1.2) by physically holding the opposing membrane at an optimal binding distance. However, longer adhesion pairs are also important for cell-cell contact formation and have been shown to result in an impaired T cell response if removed (145). When longer auxiliary molecules have been incorporated into SLBs, it is often with ICAM-1, an 18 nm long integrin which binds to LFA-1 on the cell, mimicking the formation of the immunological synapse with the TCRs accumulating in the center of the contact region and LFA-1 in the periphery (146). However, there has not been a systematic study of how, and if, the incorporation of longer adhesion molecules affects the intrinsic 2D TCR-pMHC binding.

In this chapter, Jurkat T cells are deposited onto SLBs functionalized with L3-12 TCR and differently-sized rCD2-proteins binding to pMHC (HLA-DQ8-glia-α1) and $rCD48_{T92A}$, respectively, on the surface of cells. The individual binding affinities of each protein is presented along with the protein organization in these contacts when there is a mixture of proteins in the contacts. Finally, the binding affinity of TCR is measured and presented in the presence of the differently sized rCD2 proteins.

6.2 The 2D binding affinity is influenced by the height of the protein

Here, SLBs containing POPC and 5 wt% DGS-NTA(Ni) were functionalized with three different His-tagged rCD2 proteins of varying lengths but with the same binding domain. These proteins are collectively referred to as rCD2-X (Figure 6.1A). The shortest one, rCD2-D1 is comprised of only the binding domain of rCD2 and forms a ~10 nm high complex with $rCD48_{T92A}$ (Figure 6.1A (left)) (147), $rCD2/rCD48_{T92A}$ is approximately 13 nm high and is of similar height as TCR/pMHC (Figure 6.1A (middle)) (124), whereas the longest rCD2-rCD45 protein is comprised of a rCD2 protein fused with the CD45 D1-D4 domain resulting in a ~29 nm high complex when binding $rCD48_{T92A}$ (Figure 6.1A (right)) (147).

Jurkat T cells expressing $rCD48_{T92A}$ were added to the rCD2-X functionalized SLBs and cell-SLB contact formation, as a result of protein binding, was observed for all rCD2-X proteins (Figure 6.1B). The contacts on the rCD2-D1 and rCD2 SLBs were similar, although the contacts on the rCD2 SLBs were slightly larger. However, the majority of the contacts formed by rCD2-rCD45 binding often resulted in unstable contacts that would shrink over time.

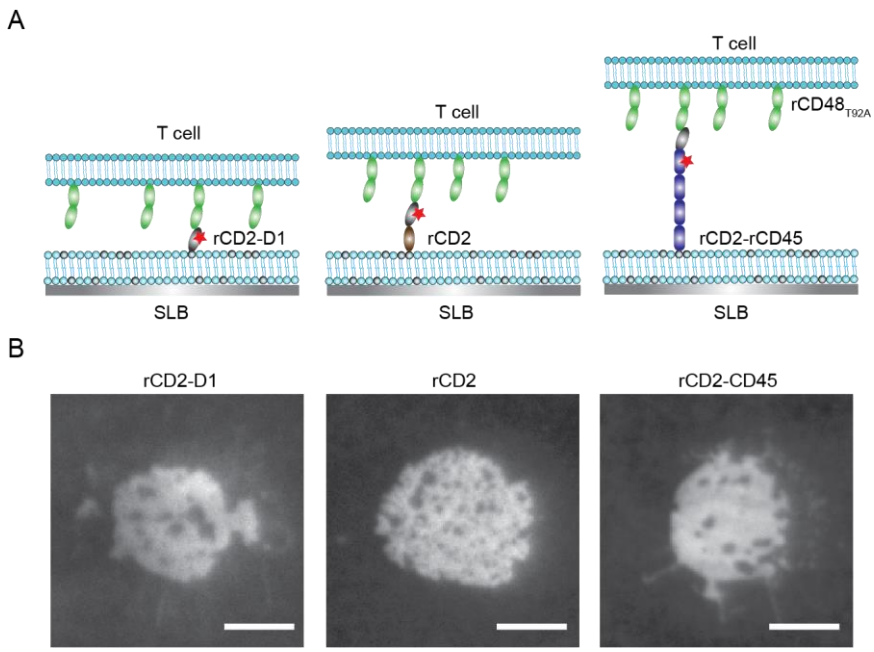

Figure 6.1. (A) Illustration of SLBs functionalized with fluorescently labelled rCD2-D1, rCD2 and rCD2-rCD45. All proteins bind to $rCD48_{T92A}$ which is expressed on the surface of the cell. **(B)** Representative fluorescence images of the cell-SLB contacts formed as a result of binding to each respective rCD2-X protein. The density of free rCD2-X in the contact region is approximately 100 molecules/μm^2. The scale bars are 5 µm.

The rCD2-X proteins were further characterized by measuring the density of bound rCD2-X proteins in the contact as a function of free proteins. All proteins showed an increasing trend of bound rCD2-X with an increasing density of free ligands in the SLB. The maximum bound density was measured to be of the order of 1000 molecules/μm^2 for all three proteins, and at a free ligand density of 100 molecules/μm^2 the bound density was approximately 600 molecules/μm^2 (Figure 6.2A), similar to what has previous been observed for rCD2 binding rCD48$_{T92A}$ (88). However, despite these similarities at high ligand densities, the 2D K_d for the rCD2-X/rCD48$_{T92A}$ interactions differed significantly. This was measured by doing single-cell Zhu-Golan analysis on between 14 to 31 different cells for each rCD2-X system. Figure 6.2B shows three representative cases, with a linear fit to each data set. From the negative reciprocal of the fits (Eq. 4.5) a 2D K_d of 5 ± 5 molecules/μm^2, 12 ± 8 molecules/μm^2 and 55 ± 41 molecules/μm^2 (median ± SD) was obtained for the rCD2/rCD48$_{T92A}$, rCD2-D1/rCD48$_{T92A}$ and rCD2-CD45/rCD48$_{T92A}$ interaction, respectively (Figure 6.2C). The rCD2/rCD48$_{T92A}$ interaction was similar to previously obtained values for ths interaction (88, 89, 91) as well as to the CD2-CD58 interaction in humans which was measured to be 5.4 – 7 molecules/μm^2 (87). Decreasing the height of rCD2 by one Ig-domain resulted in a two-fold increase of the 2D K_d, whereas a tenfold increase in 2D K_d was observed for rCD2-CD45/rCD48$_{T92A}$. By shortening the adhesion molecule, the membrane gap is decreased which compresses the glycocalyx, resulting in a net additional repulsive force (103) which could explain the weaker binding. As for rCD2-rCD45, weaker binding, and impaired cell adhesion, have previously been reported for elongated ligands (13, 148). It is possible that the weaker binding is due to a bigger conformational space of the ligand which decreases the probability of encountering a receptor to form a receptor-ligand complex. In addition, the increased flexibility and intermembrane motion of the elongated ligand is restricted upon binding. As such, there is a higher entropic penalty associated with the binding of longer proteins (108).

The density of mobile rCD48$_{T92A}$ could also be obtained from the x-intersect of the single-cell Zhu-Golan curves (Figure 6.2B) (Eq. 4.5). For the rCD2 and rCD2-D1 systems the median receptor density was 90 ± 10 molecules/μm^2 and 110 ± 17 molecules/μm^2 (median ± SE from n = 21 to 31 cells), respectively. A two-sample t-test in MATLAB revealed no significant difference between these two values. However, the rCD48$_{T92A}$ density obtained for the rCD2-rCD45 system was significantly higher 230 ± 51 molecules/μm^2 (median ± SE from n = 14 cells) (Figure 6.2B). This was significantly different from the receptor density obtained via rCD2-D1 and rCD2 ($p < 0.001$). Given that a stable cell-SLB contact is required to conduct a single cell binding affinity measurement, it stands to reason that stable rCD2-rCD45 contacts are only formed if the cell has a higher rCD48$_{T92A}$ density than the population average, in agreement with many of the cell-SLB contacts on the rCD2-rCD45 shrinking after a certain time and the cell detaching.

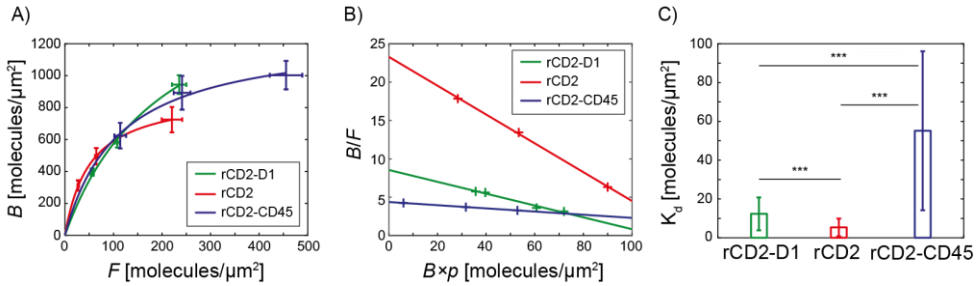

Figure 6.2. (A) The measured density of bound rCD2-X proteins in the contact, B, as a function of the free rCD2-X density in the contact, F. The data points are mean ± SE from n(rCD2-D1) = 106, n(rCD2) = 77 and n(rCD2-rCD45) = 31 cell-SLB contacts. **(B)** Three representative Zhu-Golan curves for rCD2-D1 (green), rCD2 (red) and rCD2-rCD45 (blue). The relative accumulation, B/F, is plotted against the bound ligand density, B×p. A linear fit (solid lines) is applied to the data points. **(C)** Single cell 2D K_d values for each respective rCD2-X/rCD48$_{T92A}$ interaction. The 2D K_d is given as median ± SD from n(rCD2-D1) = 21, n(rCD2) = 31 and n(rCD2-rCD45) = 14 cells. A two-sample t-test in MATLAB was used for statistical analysis with: * < 0.05, ** < 0.01, *** < 0.001.

6.3 Protein segregation in the contacts is induced by size and density differences

Next the protein organization of the cell contact was examined for SLB containing either rCD2-d1 or rCD2 as well as L3-12 TCR, labelled with Alexa Fluor 647 and Alexa Fluor 488, respectively. Jurkat T cells which expressed HLA-DQ8-glia-α1 and rCD48$_{T92A}$ were thereafter deposited onto the SLBs (Figure 6.3A). After 40 minutes of incubation time, image acquisition was performed to capture the protein distribution of each protein inside the contacts.

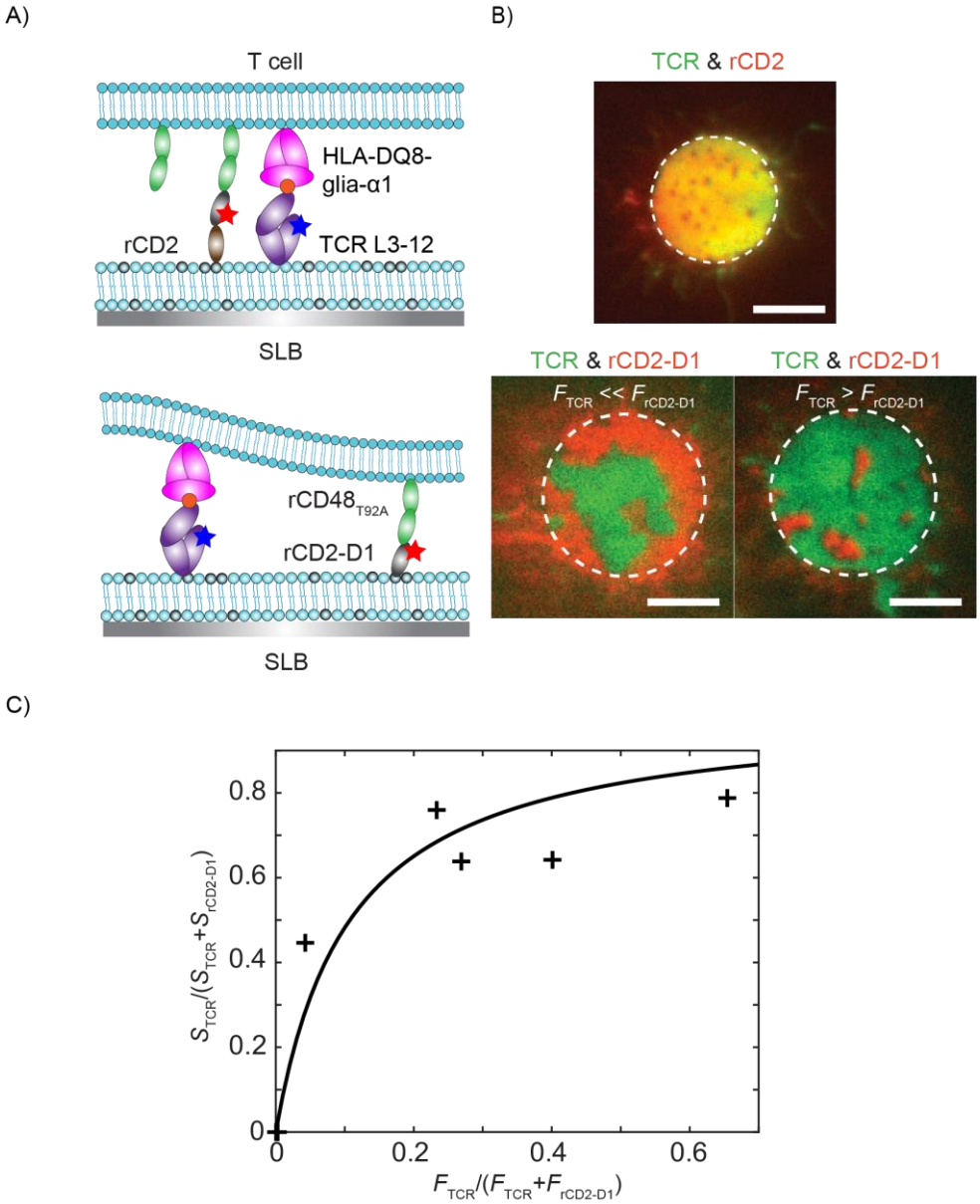

Figure 6.3. (A) Schematic illustration of HLA-DQ8-glia-α1 and rCD48$_{T92A}$ binding to SLB-anchored L3-12 TCR and rCD2 (top), and to L3-12 L3-12 TCR and rCD2-D1 (bottom). **(B)** The area fraction of the contact region occupied by TCR is plotted against the free density fraction of TCR. The data points correspond to mean values of 20-30 cell contacts. The solid line is a guide to the eye. **(C)** Representative images of (left) a cell-SLB contact containing TCR (green) and rCD2 (red), with F_{TCR} = 20 molecules/μm^2 and Fr_{CD2} = 100 molecules/μm^2, (middle) a cell-SLB contact with TCR (green) and rCD2-D1 (red), with F_{TCR} = 8 molecules/μm^2 and $F_{rCD2\text{-}D1}$ = 180 molecules/μm^2 and (right) a cell-SLB contact with TCR (green) and rCD2-D1 (red), with F_{TCR} = 16 molecules/μm^2 and $Fr_{CD2\text{-}D1}$ = 8 molecules/μm^2. The scale bar are 5 μm and the images were acquired 40 minutes after cell landing.

Clear protein segregation could be observed when TCR and rCD2-D1 were on the SLB (Figure 6.3B). This is thought to occur due to membrane-mediated repulsion to minimize cell-bending energy to accommodate the two differently-sized proteins (149–151). At lower TCR density fractions ($F_{TCR} \approx 0.1F_{rCD2\text{-}D1}$ and smaller) the contact area was largely dominated by rCD2-D1 accumulation, and vice versa for higher TCR density fractions (Figure 6.3C). The point at which both TCR and rCD2-D1 occupied 50% of the contact occurred approximately at a TCR density fraction of 0.1. The density of HLA-DQ8-glia-α1 on the cells have previously been measured to be six-fold higher than the density of $rCD48_{T92A}$ (88) which would explain why less TCR than rCD2-D1 is needed to dominate the cell-SLB contact. Although no clear colocalization could be observed between TCR and rCD2-D1, the proteins did not completely segregate from one another. TCR is still present in the more rCD2-D1 occupied areas, and vice versa, although to a lesser extent. The density ratio of bound TCR between the more heavily TCR occupied areas and the rCD2-D1 occupied areas was 1.9 ± 0.5 (mean ± SD, n = 5 separate experiments with at least 20 cell-SLB contacts per experiment). This ratio appeared to be insensitive to the density of free rCD2-D1, at least in the range $8 < F_{rCD2\text{-}D1} < 580$ molecules/μm^2. In contrast, replacing rCD2-D1 with rCD2 resulted in colocalization with TCR at all ligand densities (Figure 6.3C).

These results demonstrates how sensitive protein organization in cell contacts is to the actual protein sizes. In studies by Schmid et al. (129) and Milstein et al. (13) they found that size differences of 2 to 3 nm was sufficient to segregate or exclude proteins in the contacts (13, 129).

6.4 The 2D K_d of TCR/pMHC is affected by the density of rCD2

Although TCR and rCD2 colocalized at all examined ligand densities, the presence of auxiliary molecules in the contact region can decrease the effective affinity of the TCR-pMHC interaction (88). To further characterize this influence and how it depends on the ratio of TCR to rCD2 molecules, the 2D K_d for L3-12 TCR binding HLA-DQ8-glia-α1 was calculated for a range of different TCR and rCD2 densities. For each SLB, the average relative accumulation, B/F, of L3-12 TCR was plotted against the density of bound ligands, $B \times p$. A Zhu-Golan curve was obtained for each data point using Eq. 4.5 (Figure 6.4A), with the density of mobile HLA-DQ8-glia-α1 set to $N_{tot} \cdot f / S_{cell} = 580$ molecules/μm^2 measured previously for these cells (88). In Figure 6.4A the curves are color coded from low to high density fraction of free TCR (blue to red). Thus, the slope of the Zhu-Golan curves typically increased with the density fraction of free L3-12 TCR relative to the density of free rCD2. Since the 2D K_d is obtained from the negative reciprocal of the slope (Eq. 4.5), the

effective 2D K_d was also found to increase with an increasing density fraction of free TCR (Figure 6.4B).

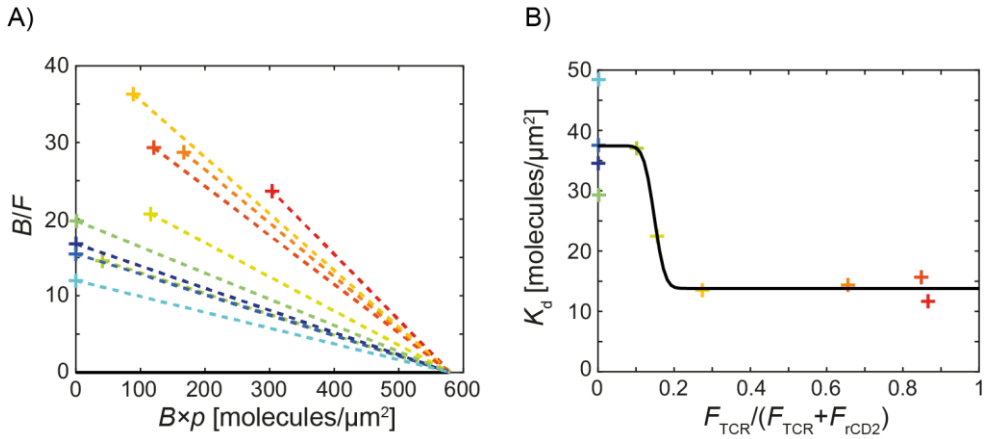

Figure 6.4. (A) The relative accumulation, B/F, of L3-12 TCR binding HLA-DQ8-glia-α1 is plotted against B×p to form corresponding Zhu-Golan curves at different densities of L3-12 TCR and rCD2 in the contact area. Individual dashed lines, intersecting the x-axis at 580 molecules/μm² is fitted to each corresponding data points (Eq. 4.5). The lines are color coded from high to low (red to blue) density fractions of free TCR. Each data point is an average from 20-30 cell-SLB contacts. **(B)** The negative reciprocal slope of the lines in (A) corresponds to the 2D K_d (Eq. 4.5) which is plotted against the density fraction of free TCR in the cell contact. The data points follow the same color coding as in (A). Each data point is derived from 20-30 cell contacts.

At low relative densities of free TCR the 2D K_d was measured to be ~37 molecules/μm², which also applies to the case when F_{TCR} < 1 molecule/μm². Increasing the density fraction of free TCRs in the contact resulted in the 2D K_d decreasing to ~14 molecules/μm², with a transition between the two regimes at approximately $F_{TCR} = 0.15(F_{TCR}+F_{rCD2})$ (Figure 6.4B). The 2D K_d at the higher TCR density fractions was similar to the effective affinity measured for L3-12 TCR binding HLA-DQ8-glia-α1 measured previously in the absence of auxiliary molecules (88).

The transition point in which the 2D K_d for TCR goes from a "low" to a "high" 2D K_d, has previously been observed to occur when the bound density of rCD2 exceeds 300 molecules/μm² (88). This is generally valid also for the data in Figure 6.4, however, not always. For example, the orange data point in Figure 6.4 had a bound rCD2 density of 700 molecules/μm², yet still the second lowest 2D K_d. The transition between the two different 2D K_d regimes instead appeared to be better related to the density fraction of TCR molecules in the SLB.

As presented in section 6.3 no clear segregation was observed for L3-12 TCR and rCD2 for all examined ligand densities. However, there could still be a local segregation not visible with diffraction limited fluorescence microscopy. When the density fraction of TCR is low rCD2/rCD48$_{T92A}$ will dominate the contact and could

act as steric hindrances for TCR/pMHC binding. To counteract the local segregation would result in an increased energy cost for binding and a higher effective 2D K_d.

6.5 The 2D K_d of TCR/pMHC is affected by the height of rCD2-X

Section 6.4 highlighted how the density of auxiliary molecules can affect the effective affinity of TCR binding pMHC. To further investigate whether the height of adhesion molecules also have an effect on this, SLBs were prepared with low densities of L3-12 TCR (F_{TCR} < 1 molecule/μm^2) and higher densities of the different rCD2-X molecules ($F_{rCD2\text{-}X}$ ≈ 100 molecules/μm^2). Due to the low density fraction of L3-12 TCR, the contact formation was dominated by rCD2-X (Figure 6.5A).

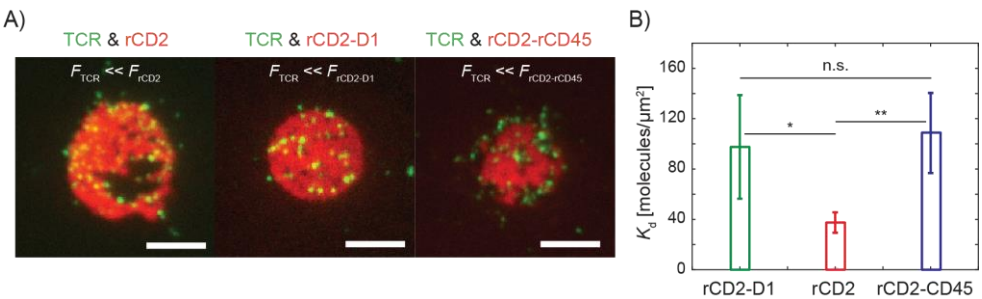

Figure 6.5. (A) Representative fluorescence images of formed cell contacts on SLBs with low densities of L3-12 TCR (F_{TCR} < 1 molecule/μm^2) (green) with (left) rCD2, (middle) rCD2-D1 and (right) rCD2-rCD45 (red). Scale bars are 5 μm. **(B)** Equation 4.5. is used to convert the accumulation of TCR in the contact to a 2D K_d for the L3-12 TCR/HLA-DQ8-glia-α1 interaction at low TCR density fractions in the presence of ~100 molecules/μm^2 rCD2-X. In the calculations, $N_{tot}{\cdot}f/S_{cell}$ = 580 molecules/μm2 (88) was used and the results are presented as mean ± SD from n = 3-4 separate experiments with 20-30 cell contacts analyzed in each experiment. A two-sample t-test in MATLAB was used for statistical analysis with: n.s. > 0.05, * < 0.05, ** < 0.01, *** < 0.001.

The 2D K_d values for L3-12 TCR binding HLA-DQ8-glia-α1 were calculated using Eq. 4.5. In the presence of ~100 free rCD2/μm^2 in the contact region, the 2D K_d for TCR was measured to be 37 ± 8 molecules/μm^2 (mean ± SD from n = 3-4 separate experiments with 20 to 30 cell-SLB contacts in each experiment) in agreement with Figure 6.4B. The 2D K_d increased to 98 ± 41 molecules/μm^2 and 109 ± 32 molecules/μm^2 (mean ± SD from n = 3-4 separate experiments with 20 to 30 cell-SLB contacts in each experiment) in the presence of rCD2-D1 and rCD2-rCD45, respectively (Figure 6.5B). The 2D K_d value for L3-12 TCR binding HLA-DQ8-glia-α1 in the presence of the height-mismatched rCD2-D1 and rCD2-rCD45 were thus ~three-fold higher compared to when the height-matched rCD2 was used.

Having the cell-SLB distance predominantly set by rCD2-X/rCD48$_{T92A}$ result in a local deformation of the cell surface from its average position above the SLB when L3-12 TCR binds HLA-DQ8-glia-α1. This results in an energy penalty for the latter interaction which in turn translates into a higher 2D K_d value. Strikingly, this energy penalty appeared to be equal for the rCD2-D1 and the rCD2-rCD45 systems, since there was no statistical difference in 2D K_d for TCR/pMHC between the two cases even though rCD2-D1/rCD48$_{T92A}$ would be more similar in height to TCR/pMHC than rCD2-CD45/rCD48$_{T92A}$. In addition, according to Monte Carlo simulations, increasing the membrane gap should have a larger influence on the binding affinity of the TCR/pMHC interaction, compared to decreasing it, because the TCR and pMHC are able to tilt to be accommodated in the smaller membrane gaps and thus still undergo binding to some degree (151). However, it is possible that the actual cell-SLB gap set by the rCD2-CD45/rCD48$_{T92A}$ interaction is smaller than that predicted from the molecular structure. For example, Milstein et al. found for a related binding system that increasing the predicted height of the binding pair by ~12 nm only resulted in a ~3 nm increase in cell-SLB gap (13).

Finally, rCD2-D1 also influenced the 2D K_d for L3-12 TCR binding HLA-DQ8-glia-α1 in the TCR-rich domains in the cell-SLB contact when having higher fractions of TCR as in Figure 6.3. As previously stated, although TCR and rCD2-D1 form separate protein domains in the cell contact the two proteins were not completely segregated, but differed in bound TCR by a factor of 1.9 under the conditions described in Section 6.3. This corresponds to a 2D K_d for L3-12 TCR/HLA-DQ8-glia-α1 in the more TCR occupied regions of 52 molecules/μm^2, which is 3.7 times higher than the 2D K_d for the same interaction in the absence of auxiliary molecules (88).

6.6 Summary

The binding of TCR to pMHC in the presence of three different adhesion pairs was studied, when the adhesion pair was (i) smaller, (ii) of similar height and (iii) larger than the height of TCR/pMHC. It was found that a height-mismatch of ~4 nm induced protein segregation in the formed cell contacts and that the 2D K_d of TCR/pMHC interaction could, at lower TCR/pMHC densities, be an order of magnitude weaker than the 2D K_d for the interaction without adhesion molecules. The influence on both protein organization in the contact and the 2D K_d of TCR/pMHC was found to depend on the density fraction of free TCR in the SLB. This was also the situation when having height-matched adhesion molecules, that colocalized with the TCR/pMHC, where the observed 2D K_d of TCR/pMHC was 2.6 times higher at low TCR density fractions relative to the density of the adhesion molecules, compared to at higher TCR density fractions. Altogether these results demonstrate the need to measure the 2D K_d of TCR-pMHC interactions in a more

complex 2D environment as the presence and the characteristics of auxiliary molecules can change the receptor-ligand binding significantly. It also indicates that the effective 2D affinity of an interaction can change significantly from the first bonds formed to an established contact containing multiple ligand-receptor bonds, a difference that can be modulated by the accumulation of other auxiliary molecules.

References

1. Murphy, K., and C. Weaver. 2017. Janeway's Immunobiology 9th edition. Garland Science.
2. Davis, M.M., and Y. hsiu Chien. 1995. Issues concerning the nature of antigen recognition by αβ and γδ T-cell receptors. *Immunol. Today*. 16:316–318.
3. Lawand, M., J. Déchanet-Merville, and M.C. Dieu-Nosjean. 2017. Key features of gamma-delta T-cell subsets in human diseases and their immunotherapeutic implications. *Front. Immunol.* 8.
4. Davis, M.M., J.J. Boniface, Z. Reich, D. Lyons, J. Hampl, B. Arden, and Y. Chien. 1998. Ligand Recognition By Aβ T Cell Receptors. *Annu. Rev. Immunol.* 16:523–544.
5. Alam, S.M., P.J. Travers, J.L. Wung, W. Nasholds, S. Redpath, S.C. Jameson, and N.R.J. Gascoigne. 1996. T cell-receptor affinity and thymocyte positive selection. *Nature*. 381:616–620.
6. Davis, S.J., and P.A. Van Der Merwe. 1996. The structure and ligand interactions of CD2: Implications for T-cell function. *Immunol. Today*. 17:177–187.
7. Binder, C., F. Cvetkovski, F. Sellberg, S. Berg, H. Paternina Visbal, D.H. Sachs, E. Berglund, and D. Berglund. 2020. CD2 Immunobiology. *Front. Immunol.* 11:1–14.
8. Bierer, B.E., and S.J. Burakoff. 1988. T cell adhesion molecules. 2584–2590.
9. Dustin, M.L., L.M. Ferguson, P.Y. Chan, T.A. Springer, and D.E. Golan. 1996. Visualization of CD2 interaction with LFA-3 and determination of the two-Dimensional dissociation constant for adhesion receptors in a contact area. *J. Cell Biol.* 132:465–474.
10. Anton van der Merwe, P., P.N. McNamee, E.A. Davies, A.N. Barclay, and S.J. Davis. 1995. Topology of the CD2-CD48 cell-adhesion molecule complex: implications for antigen recognition by T cells. *Curr. Biol.* 5:74–84.
11. Dustin, M.L., D.E. Golan, D. Zhu, J.M. Miller, W. Meier, E.A. Davies, and P.A. Van Der Merwe. 1997. Low Affinity Interaction of Human or Rat T Cell Adhesion Molecule CD2 with Its Ligand Aligns Adhering Membranes to Achieve High Physiological Affinity *. 272:30889–30898.
12. Gückel, B., C. Berek, M. Lutz, P. Altevogt, V. Schirrmacher, and B.A. Kyewski. 1991. Anti-CD2 antibodies induce T cell unresponsiveness in vivo. *J. Exp. Med.* 174:957–967.
13. Milstein, O., S.-Y.Y. Tseng, T. Starr, J. Llodra, A. Nans, M. Liu, M.K. Wild, P.A. Van Der Merwe, D.L. Stokes, Y. Reisner, and M.L. Dustin. 2008. Nanoscale increases in CD2-CD48-mediated intermembrane spacing decrease adhesion and reorganize the immunological synapse. *J. Biol. Chem.* 283:34414–34422.

14. Wang, J.H., A. Smolyar, K. Tan, J.H. Liu, M. Kim, Z.Y.J. Sun, G. Wagner, and E.L. Reinherz. 1999. Structure of a heterophilic adhesion complex between the human CD2 and CD58 (LFA-3) counterreceptors. *Cell*. 97:791–803.
15. Dustin, M.L., and A.C. Chan. 2000. Signaling takes shape in the immune system. *Cell*. 103:283–294.
16. Symons, A., A.C. Willis, and A.N. Barclay. 1999. Domain organization of the extracellular region of CD45. *Protein Eng.* 12:885–892.
17. Holmes, N. 2006. CD45: All is not yet crystal clear. *Immunology*. 117:145–155.
18. Junghans, V., J. Hladilkova, A.M. Santos, M. Lund, P. Jönsson, S.J. Davis, and P. Jönsson. 2018. Hydrodynamic trapping measures the interaction between membrane-associated molecules. *Sci. Rep.* 8:12479.
19. Barclay, A.N., and A.. Williams. 1986. Handbook of Experimental Immunology. Blackwell Scientific Publications.
20. Chang, V.T., R.A. Fernandes, K.A. Ganzinger, S.F. Lee, C. Siebold, J. McColl, P. Jönsson, M. Palayret, K. Harlos, C.H. Coles, E.Y. Jones, Y. Lui, E. Huang, R.J.C. Gilbert, D. Klenerman, A.R. Aricescu, and S.J. Davis. 2016. Initiation of T cell signaling by CD45 segregation at "close contacts." *Nat. Immunol.* 17:574–582.
21. Hermiston, M.L., Z. Xu, and A. Weiss. 2003. CD45: A Critical Regulator of Signaling Thresholds in Immune Cells. *Annu. Rev. Immunol.* 21:107–137.
22. Courtney, A.H., A.A. Shvets, W. Lu, G. Griffante, M. Mollenauer, V. Horkova, W.L. Lo, S. Yu, O. Stepanek, A.K. Chakraborty, and A. Weiss. 2019. CD45 functions as a signaling gatekeeper in T cells. *Sci. Signal.* 12.
23. Singer, S.J.J., and G.L.L. Nicolson. 1972. The fluid mosaic model of the structure of cell membranes. *Science (80-.).* 175:720–731.
24. Alberts, B., D. Bray, K. Hopkin, A. John, J. Lewis, M. Raff, K. Roberts, and P. Walter. 2013. Essential Cell Biology Fourth Edition. Garland Science.
25. Ti Tien, H., and A. Ottova-Leitmannova. 2000. Membrane Biophysics: As Viewed from Experimental Bilayer Lipid Membranes. Elsevier.
26. Alberts, B., A. Johnson, J. Lewis, M. Raff, K. Roberts, and P. Walter. 2002. Molecular Biology of the Cell. 4th edition. Garland Science.
27. Edidin, M. 2003. Lipids on the frontier: A century of cell-membrane bilayers. *Nat. Rev. Mol. Cell Biol.* 4:414–418.
28. Tamm, L.K., H.M. Mcconnell, S. Laboratoryfor, and P. Chemistry. 1985. Supported Phospholipid Bilayers. *Biophys. J.* 47:105–113.
29. Crites, T.J., M. Maddox, K. Padhan, J. Muller, C. Eigsti, R. Varma, I. Diseases, M.P. Program, B. Medicine, F.C. Section, and I. Diseases. 2016. Supported Lipid Bilayer Technology for the Study of Cellular Interfaces. .
30. Osborn, T.D., and P. Yager. 1995. Formation of Planar Solvent-Free Phospholipid Bilayers by Langmuir-Blodgett Transfer of Monolayers to Micromachined Apertures in Silicon. *Langmuir*. 11:8–12.
31. Simonsen, A.C., and L.A. Bagatolli. 2004. Structure of spin-coated lipid films and domain formation in supported membranes formed by hydration. *Langmuir*. 20:9720–9728.

32. Reimhult, E., B. Kasemo, and F. Höök. 2009. Rupture pathway of phosphatidylcholine liposomes on silicon dioxide. *Int. J. Mol. Sci.* 10:1683–1696.
33. Reimhult, E., F. Höök, and B. Kasemo. 2003. Intact vesicle adsorption and supported biomembrane formation from vesicles in solution: Influence of surface chemistry, vesicle size, temperature, and osmotic pressure. *Langmuir*. 19:1681–1691.
34. Castellana, E.T., and P.S. Cremer. 2006. Solid supported lipid bilayers: From biophysical studies to sensor design. *Surf. Sci. Rep.* 61:429–444.
35. Richter, R.P., R. Bérat, and A.R. Brisson. 2006. Formation of solid-supported lipid bilayers: An integrated view. *Langmuir*. 22:3497–3505.
36. Reviakine, I., and A. Brisson. 2000. Formation of supported phospholipid bilayers from unilamellar vesicles investigated by atomic force microscopy. *Langmuir*. 16:1806–1815.
37. Johnson, J.M., T. Ha, S. Chu, and S.G. Boxer. 2002. Early steps of supported bilayer formation probed by single vesicle fluorescence assays. *Biophys. J.* 83:3371–3379.
38. Salafsky, J., J.T. Groves, and S.G. Boxer. 1996. Architecture and function of membrane proteins in planar supported bilayers: A study with photosynthetic reaction centers. *Biochemistry*. 35:14773–14781.
39. Winterhalter, M. 2000. Black lipid membranes. *Curr. Opin. Colloid Interface Sci.* 5:250–255.
40. Tanaka, M., and E. Sackmann. 2005. Polymer-supported membranes as models of the cell surface. *Nature*. 437:656–663.
41. Chan, Y.H.M., and S.G. Boxer. 2007. Model membrane systems and their applications. *Curr. Opin. Chem. Biol.* 11:581–587.
42. Wagner, M.L., and L.K. Tamm. 2000. Tethered polymer-supported planar lipid bilayers for reconstitution of integral membrane proteins: Silane-polyethyleneglycol-lipid as a cushion and covalent linker. *Biophys. J.* 79:1400–1414.
43. Kaufmann, S., G. Papastavrou, K. Kumar, M. Textor, and E. Reimhult. 2009. A detailed investigation of the formation kinetics and layer structure of poly(ethylene glycol) tether supported lipid bilayers. *Soft Matter*. 5:2804–2814.
44. Kuhl, T.L., D.E. Leckband, D.D. Lasic, and J.N. Israelachvili. 1994. Modulation of interaction forces between bilayers exposing short-chained ethylene oxide headgroups. *Biophys. J.* 66:1479–1488.
45. Paulick, M.G., A.R. Wise, M.B. Forstner, J.T. Groves, and C.R. Bertozzi. 2007. Synthetic analogues of glycosylphosphatidylinositol-anchored proteins and their behavior in supported lipid bilayers. *J. Am. Chem. Soc.* 129:11543–11550.
46. Paulick, M.G., and C.R. Bertozzi. 2008. The glycosylphosphatidylinositol anchor: A complex membrane-anchoring structure for proteins. *Biochemistry*. 47:6991–7000.
47. Yu, C.H., and J.T. Groves. 2010. Engineering supported membranes for cell biology. *Med. Biol. Eng. Comput.* 48:955–963.
48. Dustin, M.L., and J.T. Groves. 2012. Receptor signaling clusters in the immune synapse. *Annu. Rev. Biophys.* 41:543–556.
49. Nye, J.A., and J.T. Groves. 2008. Kinetic Control of Histidine-Tagged Protein Surface Density on Supported Lipid Bilayers. 11820–11824.

50. Lichtman, J.W., and J.A. Conchello. 2005. Fluorescence microscopy. *Nat. Methods*. 2:910–919.
51. Heit, B. 2011. Fluorescent Microscopy. .
52. Herman, B. 2002. Fluorescence Microscopy. *Curr. Protoc. Cell Biol.* 1–10.
53. Petty, H.R. 2007. Fluorescence microscopy: Established and emerging methods, experimental strategies, and applications in immunology. *Microsc. Res. Tech.* 70:687–709.
54. Fish, K.N. 2009. Total internal reflection fluorescence (TIRF) microscopy. *Curr. Protoc. Cytom.* 1–13.
55. Mantil, E., T. Crippin, A. Ianoul, and T.J. Avis. 2017. Experimental parameters leading to optimal bilayers for total internal reflection fluorescence microscopy visualization. *Microsc. Microanal.* 23:97–112.
56. Axelrod, D., D.E. Koppel, J. Schlessinger, E. Elson, and W.W. Webb. 1976. Mobility measurement by analysis of fluorescence photobleaching recovery kinetics. *Biophys. J.* 16:1055–1069.
57. Lopez, A., L. Dupou, A. Altibelli, J. Trotard, and J.F. Tocanne. 1988. Fluorescence recovery after photobleaching (FRAP) experiments under conditions of uniform disk illumination. Critical comparison of analytical solutions, and a new mathematical method for calculation of diffusion coefficient D. *Biophys. J.* 53:963–970.
58. Jönsson, P., M.P. Jonsson, J.O. Tegenfeldt, and F. Höök. 2008. A method improving the accuracy of fluorescence recovery after photobleaching analysis. *Biophys. J.* 95:5334–5348.
59. Tolentino, T.P., J. Wu, V.I. Zarnitsyna, Y. Fang, M.L. Dustin, and C. Zhu. 2008. Measuring Diffusion and Binding Kinetics by Contact Area FRAP. *Biophys. J.* 95:920–930.
60. Carrero, G., D. McDonald, E. Crawford, G. De Vries, and M.J. Hendzel. 2003. Using FRAP and mathematical modeling to determine the in vivo kinetics of nuclear proteins. *Methods*. 29:14–28.
61. Merwe, P.A. Van Der. 2010. Surface plasmon resonance GENERAL PRINCIPLES OF BIACORE EXPERIMENTS. *Physics (College. Park. Md).*
62. Van Der Merwe, P.A., and A.N. Barclay. 1996. Analysis of cell-adhesion molecule interactions using surface plasmon resonance. *Curr. Opin. Immunol.* 8:257–261.
63. Stone, J.D., A.S. Chervin, and D.M. Kranz. 2009. T-cell receptor binding affinities and kinetics: impact on T-cell activity and specificity. *Immunology*. 126:165–176.
64. Robert, P., M. Aleksic, O. Dushek, V. Cerundolo, P. Bongrand, and P.A. Van Der Merwe. 2012. Kinetics and mechanics of two-dimensional interactions between T cell receptors and different activating ligands. *Biophys. J.* 102:248–257.
65. Edwards, L.J., V.I. Zarnitsyna, J.D. Hood, B.D. Evavold, and C. Zhu. 2012. Insights into T cell recognition of antigen: Significance of two-dimensional kinetic parameters. *Front. Immunol.* 3:1–9.
66. Bell, G.I. 1978. Models for the specific adhesion of cells to cells. *Science (80-.).* 200:618–627.

67. Carrasco, Y.R., S.J. Fleire, T. Cameron, M.L. Dustin, F.D. Batista, and I. Fields. 2004. LFA-1 / ICAM-1 Interaction Lowers the Threshold of B Cell Activation by Facilitating B Cell Adhesion and Synapse Formation. 20:589–599.

68. Moingeon, P., H. Chang, B.P. Wallner, C. Stebbins, A.Z. Frey, and E.L. Reinherz. 1989. CD2-mediated adhesion facilitates. 339:312–314.

69. Davis, S.J., and P.A. van der Merwe. 2006. The kinetic-segregation model: TCR triggering and beyond. *Nat. Immunol.* 7:803–809.

70. Kaizuka, Y., A.D. Douglass, R. Varma, M.L. Dustin, and R.D. Vale. 2007. Mechanisms for segregating T cell receptor and adhesion molecules during immunological synapse formation in Jurkat T cells. .

71. Deeg, J., M. Axmann, J. Matic, A. Liapis, D. Depoil, J. Afrose, S. Curado, M.L. Dustin, and J.P. Spatz. 2013. T cell activation is determined by the number of presented antigens. *Nano Lett.* 13:5619–5626.

72. Manz, B.N., B.L. Jackson, R.S. Petit, M.L. Dustin, and J. Groves. 2011. T-cell triggering thresholds are modulated by the number of antigen within individual T-cell receptor clusters. *Proc. Natl. Acad. Sci. U. S. A.* 108:9089–9094.

73. Huang, J., V.I. Zarnitsyna, B. Liu, L.J. Edwards, N. Jiang, B.D. Evavold, and C. Zhu. 2010. The kinetics of two-dimensional TCR and pMHC interactions determine T-cell responsiveness. *Nature*. 464:932–936.

74. Chesla, S.E., P. Selvaraj, and C. Zhu. 1998. Measuring two-dimensional receptor-ligand binding kinetics by micropipette. *Biophys. J.* 75:1553–1572.

75. Dam, T., M. Chouliara, V. Junghans, and P. Jönsson. 2022. Supported Lipid Bilayers and the Study of Two-Dimensional Binding Kinetics. *Front. Mol. Biosci.* 9:1–15.

76. Liu, B., W. Chen, B.D.D. Evavold, and C. Zhu. 2014. Accumulation of Dynamic Catch Bonds between TCR and Agonist Peptide-MHC Triggers T Cell Signaling. *Cell*. 157:357–368.

77. Alon, R., S. Chen, K.D. Puri, E.B. Finger, and T.A. Springer. 1997. The kinetics of L-selectin tethers and the mechanics of selectin- mediated rolling. *J. Cell Biol.* 138:1169–1180.

78. Huse, M. 2017. Mechanical forces in the immune system. *Nat. Rev. Immunol.* 17:679–690.

79. Wang, Y., J. Yan, and B.T. Goult. 2019. Force-Dependent Binding Constants. *Biochemistry*. 58:4696–4709.

80. Hong, J., S.P. Persaud, S. Horvath, P.M. Allen, B.D. Evavold, and C. Zhu. 2015. Force-Regulated In Situ TCR–Peptide-Bound MHC Class II Kinetics Determine Functions of CD4 + T Cells. *J. Immunol.* 195:3557–3564.

81. Sibener, L. V, R.A. Fernandes, E.M. Kolawole, B.D. Evavold, R.D. Vale, K.C. Garcia, L. V Sibener, R.A. Fernandes, E.M. Kolawole, C.B. Carbone, and F. Liu. 2018. Isolation of a Structural Mechanism for Uncoupling Article Isolation of a Structural Mechanism for Uncoupling T Cell Receptor Signaling from Peptide-MHC Binding. *Cell*. 174:672-687.e27.

82. Mckeithan, T.W. 1995. Kinetic proofreading in T-cell receptor signal transduction. *Proc. Natl. Acad. Sci. U. S. A.* 92:5042–5046.

83. Limozin, L., M. Bridge, P. Bongrand, O. Dushek, P.A. van der Merwe, and P. Robert. 2019. TCR–pMHC kinetics under force in a cell-free system show no intrinsic catch bond, but a minimal encounter duration before binding. *Proc. Natl. Acad. Sci. U. S. A.* 116:16943–16948.

84. Huang, D. L., Bax, N. A., Buckley, C. D., Weis, W. I., and D., and A. R. 2017. Vinculin forms a directionally asymmetric catch bond with F-actin. *Science (80-.).* 357:703–706.

85. Huang, J., C. Meyer, and C. Zhu. 2012. T cell antigen recognition at the cell membrane. *Mol. Immunol.* 52:155–164.

86. Zhang, Y., G. Sun, S. Lü, N. Li, and M. Long. 2008. Low spring constant regulates P-selectin-PSGL-1 bond rupture. *Biophys. J.* 95:5439–5448.

87. Zhu, D.-M., M.L. Dustin, C.W. Cairo, and D.E. Golan. 2007. Analysis of Two-Dimensional Dissociation Constant of Laterally Mobile Cell Adhesion Molecules. *Biophys. J.* 92:1022–1034.

88. Junghans, V., M. Chouliara, A.M. Santos, D. Hatherley, J. Petersen, T. Dam, L.M. Svensson, J. Rossjohn, S.J. Davis, and P. Jönsson. 2020. Effects of a local auxiliary protein on the two-dimensional affinity of a TCR-peptide MHC interaction. *J. Cell Sci.* 133:jcs.245985.

89. Dam, T., V. Junghans, J. Humphrey, M. Chouliara, and P. Jönsson. 2021. Calcium Signaling in T Cells Is Induced by Binding to Nickel-Chelating Lipids in Supported Lipid Bilayers. *Front. Physiol.* 11:1–8.

90. Bromley, S.K., A. Iaboni, S.J. Davis, A. Whitty, J.M. Green, A.S. Shaw, A. Weiss, and M.L. Dustin. 2001. The immunological synapse and CD28-CD80 interactions. *Nat. Immunol.* 2:1159–1166.

91. Chouliara, M., V. Junghans, T. Dam, A.M. Santos, S.J. Davis, and P. Jönsson. 2021. Single-cell measurements of two-dimensional binding affinity across cell contacts. *Biophys. J.* 120:1–9.

92. Mege, J.-L., C. Capo, A.-M. Benoliel, C. Foa, R. Galindo, and P. Bongrand. 1986. Quantification of cell surface roughness; a method for studying cell mechanical and adhesive properties. *J. Theor. Biol.* 119:147–160.

93. Dushek, O., R. Das, and D. Coombs. 2008. Analysis of membrane-localized binding kinetics with FRAP. *Eur. Biophys. J.* 37:627–638.

94. Wu, J., Y. Fang, V.I. Zarnitsyna, T.P. Tolentino, M.L. Dustin, and C. Zhu. 2008. A coupled diffusion-kinetics model for analysis of contact-area FRAP experiment. *Biophys. J.* 95:910–919.

95. Jönsson, P., J.H. Southcombe, A.M. Santos, J. Huo, R.A. Fernandes, J. McColl, M. Lever, E.J. Evans, A. Hudson, V.T. Chang, T.T.T. Hanke, A. Godkin, P.D. Dunne, M.H. Horrocks, M. Palayret, G.R. Screaton, J. Petersen, J. Rossjohn, L. Fugger, O. Dushek, X.-N. Xu, S.J. Davis, D. Klenerman, P. Jonsson, J.H. Southcombe, A.M. Santos, J. Huo, R.A. Fernandes, J. McColl, M. Lever, E.J. Evans, A. Hudson, V.T. Chang, T.T.T. Hanke, A. Godkin, P.D. Dunne, M.H. Horrocks, M. Palayret, G.R. Screaton, J. Petersen, J. Rossjohn, L. Fugger, O. Dushek, X.-N. Xu, S.J. Davis, and D. Klenerman. 2016. Remarkably low affinity of CD4/peptide-major histocompatibility complex class II protein interactions. *Proc. Natl. Acad. Sci. U. S. A.* 113:5682–5687.

96. Manzo, C., and M.F. Garcia-Parajo. 2015. A review of progress in single particle tracking: From methods to biophysical insights. *Reports Prog. Phys.*

97. Axmann, M., J.B. Huppa, M.M. Davis, and G.J. Schütz. 2012. Determination of interaction kinetics between the T cell receptor and peptide-loaded MHC class II via single-molecule diffusion measurements. *Biophys. J.* 103:17–19.

98. O'Donoghue, G.P., R.M. Pielak, A.A. Smoligovets, J.J. Lin, J.T. Groves, G.P.O. Donoghue, R.M. Pielak, A.A. Smoligovets, J.J. Lin, J.T. Groves, U. States, P.B. Division, L. Berkeley, G.P. O'Donoghue, R.M. Pielak, A.A. Smoligovets, J.J. Lin, and J.T. Groves. 2013. Direct single molecule measurement of TCR triggering by agonist pMHC in living primary T cells. *Elife*. 2:1–16.

99. Jares-Erijman, E.A., and T.M. Jovin. 2003. FRET imaging. *Nat. Biotechnol.* 21:1387–1395.

100. Bajar, B.T., E.S. Wang, S. Zhang, M.Z. Lin, and J. Chu. 2016. A guide to fluorescent protein FRET pairs. *Sensors (Switzerland)*. 16:1–24.

101. Huppa, J.B., M. Axmann, M.A. Mörtelmaier, B.F. Lillemeier, E.W. Newell, M. Brameshuber, L.O. Klein, G.J. Schütz, and M.M. Davis. 2010. TCR-peptide-MHC interactions in situ show accelerated kinetics and increased affinity. *Nature*. 463:963–967.

102. Lin, J.J.Y., S.T. Low-Nam, K.N. Alfieri, D.B. McAffee, N.C. Fay, J.T. Groves, D.B.M. Jenny J. Y. Lin*, Shalini T. Low-Nam*, Katherine N. Alfieri†, and J.T.G. Nicole C. Fay‡. 2019. Mapping the stochastic sequence of individual ligand-receptor binding events to cellular activation: T cells act on the rare events. *Sci. Signal.* 12:1–14.

103. Bell, G.I., M. Dembo, and P. Bongrand. 1984. Cell adhesion. Competition between nonspecific repulsion and specific bonding. *Biophys. J.* 45:1051–1064.

104. Dustin, M.L., S.K. Bromley, M.M. Davis, and C. Zhu. 2001. Identification of Self Through Two-Dimensional Chemistry and Synapses. *Annu. Rev. Cell Dev. Biol.* 17:133–157.

105. Weikl, T.R., J. Hu, G.K. Xu, and R. Lipowsky. 2016. Binding equilibrium and kinetics of membrane-anchored receptors and ligands in cell adhesion: Insights from computational model systems and theory. *Cell Adhes. Migr.* 10:576–589.

106. Hu, J., R. Lipowsky, and T.R. Weikl. 2013. Binding constants of membrane-anchored receptors and ligands depend strongly on the nanoscale roughness of membranes. *Proc. Natl. Acad. Sci.*

107. Krobath, H., B. Rózycki, R. Lipowsky, and T.R. Weikl. 2009. Binding cooperativity of membrane adhesion receptors. *Soft Matter*. 5:3354–3361.

108. Wu, Y., J. Vendome, L. Shapiro, A. Ben-Shaul, and B. Honig. 2011. Transforming binding affinities from three dimensions to two with application to cadherin clustering. *Nature*. 475:510–513.

109. Abraham, R.T., and A. Weiss. 2017. Jurkat T cells and development of the T-cell receptor signalling paradigm 01 2017/5/1. *Nat. Rev. Immunol.* 4:1–8.

110. Malissen, B., and P. Bongrand. 2015. Early T Cell Activation: Integrating Biochemical, Structural, and Biophysical Cues. *Annu. Rev. Immunol.* 33:539–561.

111. Mørch, A.M., Š. Bálint, A.M. Santos, S.J. Davis, and M.L. Dustin. 2020. Coreceptors and TCR Signaling – the Strong and the Weak of It. *Front. Cell Dev. Biol.* 8:1–13.

112. Lillemeier, B.F., M.A. Mörtelmaier, M.B. Forstner, J.B. Huppa, J.T. Groves, and M.M. Davis. 2010. TCR and Lat are expressed on separate protein islands on T cell membranes and concatenate during activation. *Nat. Immunol.* 11:90–96.

113. Irvine, D.J., M.A. Purbhoo, M. Krogsgaard, and M.M. Davis. 2002. Direct observation of ligand recognition by T cells. *Nature*. 419:845–849.

114. Morris, G.P., and P.M. Allen. 2012. How the TCR balances sensitivity and specificity for the recognition of self and pathogens. *Nat. Immunol.* 13:121–128.

115. Ma, Z., K.A. Sharp, P.A. Janmey, and T.H. Finkel. 2008. Surface-anchored monomeric agonist pMHCs alone trigger TCR with high sensitivity. *PLoS Biol.* 6:0328–0342.

116. Matsui, K., J.J. Boniface, P. Steffner, P.A. Reay, and M.M. Davis. 1994. Kinetics of T-cell receptor binding to peptide/I-E(k) complexes: Correlation of the dissociation rate with T-cell responsiveness. *Proc. Natl. Acad. Sci. U. S. A.* 91:12862–12866.

117. Lyons, D.S., S.A. Lieberman, J. Hampl, J.J. Boniface, Y.H. Chien, L.J. Berg, and M.M. Davis. 1996. A TCR binds to antagonist ligands with lower affinities and faster dissociation rates than to agonists. *Immunity*. 5:53–61.

118. S., V., M. S., C. M., P. E., and L. A. 1995. Serial triggering of many T-cell receptors by a few peptide-MHC complexes. *Nature*. 375:148–151.

119. Chakraborty, Arup K. Weiss, A. 2014. Insights into the initiation of TCR signaling. *Nat. Immunol.* 15:798–807.

120. Kalergis, A.H., N. Boucheron, M.A. Doucey, E. Palmieri, E.C. Goyarts, Z. Vegh, I.F. Luescher, and S.G. Nathenson. 2001. Efficient T cell activation requires an optimal dwell-time of interaction between the TCR and the pMHC complex. *Nat. Immunol.* 2:229–234.

121. Merwe, P.A. Van Der, and O. Dushek. 2010. Mechanisms for T cell receptor triggering. *Nat. Publ. Gr.* 11:47–55.

122. Gil, D., A.G. Schrum, B. Alarcón, and E. Palmer. 2005. T cell receptor engagement by peptide - MHC ligands induces a conformational change in the CD3 complex of thymocytes. *J. Exp. Med.* 201:517–522.

123. Krogsgaard, M., Q.J. Li, C. Sumen, J.B. Huppa, M. Huse, and M.M. Davis. 2005. Agonist/endogenous peptide-MHC heterodimers drive T cell activation and sensitivity. *Nature*. 434:238–243.

124. Choudhuri, K., D. Wiseman, M.H. Brown, K. Gould, and P.A. Van Der Merwe. 2005. T-cell receptor triggering is critically dependent on the dimensions of its peptide-MHC ligand. 436.

125. Irles, C., A. Symons, F. Michel, T.R. Bakker, P.A. van der Merwe, and O. Acuto. 2003. CD45 ectodomain controls interaction with GEMs and Lck activity for optimal TCR signaling. *Nat. Immunol.* 4:189–197.

126. Cordoba, S.P., K. Choudhuri, H. Zhang, M. Bridge, A.B. Basat, M.L. Dustin, and P.A. van der Merwe. 2013. The large ectodomains of CD45 and CD148 regulate their segregation from and inhibition of ligated T-cell receptor. *Blood*. 121:4295–4302.

127. James, J.R., and R.D. Vale. 2012. Biophysical mechanism of T-cell receptor triggering in a reconstituted system. *Nature*. 487:64–69.

128. Lin, J., and A. Weiss. 2003. The tyrosine phosphatase CD148 is excluded from the immunologic synapse and down-regulates prolonged T cell signaling. *J. Cell Biol.* 162:673–682.

129. Schmid, E.M.M., M.H.H. Bakalar, K. Choudhuri, J. Weichsel, H.S.H. Ann, P.L.L. Geissler, M.L.L. Dustin, and D.A.A. Fletcher. 2017. Size-dependent protein segregation at membrane interfaces. *Nat. Phys.* 12:704–711.

130. Bunnell, S.C., D.I. Hong, J.R. Kardon, T. Yamazaki, C.J. McGlade, V.A. Barr, and L.E. Samelson. 2002. T cell receptor ligation induces the formation of dynamically regulated signaling assemblies. *J. Cell Biol.* 158:1263–1275.

131. Al-Aghbar, M.A., Y.-S. Chu, B.-M. Chen, and S.. Roffler. 2018. High-Affinity Ligands Can Trigger T Cell Receptor Signaling Without CD45 Segregation. 9.

132. Roffler, S.R. 2017. The affinity of elongated Membrane-Tethered ligands Determines Potency of T cell receptor Triggering. 8:1–21.

133. Al-Aghbar, M.A., A.K. Jainarayanan, M.L. Dustin, and S.R. Roffler. 2022. The interplay between membrane topology and mechanical forces in regulating T cell receptor activity. *Commun. Biol.* 5:1–16.

134. Fernandes, R.A., K.A. Ganzinger, J.C. Tzou, P. Jönsson, S.F. Lee, M. Palayret, A.M. Santos, A.R. Carr, A. Ponjavic, V.T. Chang, C. Macleod, B. Christoffer Lagerholm, A.E. Lindsay, O. Dushek, A. Tilevik, S.J. Davis, and D. Klenerman. 2019. A cell topography-based mechanism for ligand discrimination by the T cell receptor. *Proc. Natl. Acad. Sci. U. S. A.* 116:14002–14010.

135. Lippert, A.H., I.B. Dimov, A.K. Winkel, J. Humphrey, J. McColl, K.Y. Chen, A.M. Santos, E. Jenkins, K. Franze, S.J. Davis, and D. Klenerman. 2021. Soft Polydimethylsiloxane-Supported Lipid Bilayers for Studying T Cell Interactions. *Biophys. J.* 120:35–45.

136. Santos, A.M., A. Ponjavic, M. Fritzsche, R.A. Fernandes, J.B. Serna, M.J. Wilcock, F. Schneider, I. Urbančič, J. Mccoll, C. Anzilotti, K.A. Ganzinger, M. Aßmann, D. Depoil, R.J. Cornall, M.L. Dustin, D. Klenerman, S.J. Davis, C. Eggeling, and S.F. Lee. 2018. Capturing resting T cells: the perils of PLL. *Nat. Immunol.* 19:203–205.

137. Sage, P.T., L.M. Varghese, R. Martinelli, T.E. Sciuto, M. Kamei, A.M. Dvorak, T.A. Springer, A.H. Sharpe, and C. V. Carman. 2012. Antigen Recognition Is Facilitated by Invadosome-like Protrusions Formed by Memory/Effector T Cells. *J. Immunol.* 188:3686–3699.

138. Cai, E., K. Marchuk, P. Beemiller, C. Beppler, M.G. Rubashkin, V.M. Weaver, A. Gérard, T.-L. Liu, B.-C. Chen, E. Betzig, F. Bartumeus, and M.F. Krummel. 2017. Visualizing dynamic microvillar search and stabilization during ligand detection by T cells. *Science*. 356:eaal3118.

139. Fölser, M., V. Motsch, R. Platzer, J.B. Huppa, and G.J. Schütz. 2021. A Multimodal Platform for Simultaneous T-Cell Imaging, Defined Activation, and Mechanobiological Characterization. *Cells*. 10:1–12.

140. Taylor, M.J., K. Husain, Z.J. Gartner, S. Mayor, R.D. Vale, M.J. Taylor, K. Husain, Z.J. Gartner, S. Mayor, and R.D. Vale. 2017. A DNA-Based T Cell Receptor Reveals a Role for Receptor Clustering in Ligand Discrimination. *Cell*. 169:108.e1-108.e20.
141. Yokosuka, T., W. Kobayashi, K. Sakata-Sogawa, M. Takamatsu, A. Hashimoto-Tane, M.L. Dustin, M. Tokunaga, and T. Saito. 2008. Spatiotemporal Regulation of T Cell Costimulation by TCR-CD28 Microclusters and Protein Kinase C θ Translocation. *Immunity*. 29:589–601.
142. Lippert, A.H., I.B. Dimov, A. Winkel, J. Mccoll, J. Humphrey, K.Y. Chen, A.M. Santos, E. Jenkins, K. Franze, S.J. Davis, and D. Klenerman. 2020. Robust T-cell signaling triggered on soft polydimethylsiloxane-supported lipid-bilayers 1 2. .
143. Ponjavic, A., J. McColl, A.R. Carr, A.M. Santos, K. Kulenkampff, A. Lippert, S.J. Davis, D. Klenerman, and S.F. Lee. 2018. Single-Molecule Light-Sheet Imaging of Suspended T Cells. *Biophys. J.* 114.
144. Chen, K.Y., E. Jenkins, M. Körbel, A. Ponjavic, A.H. Lippert, A.M. Santos, N. Ashman, C. O'Brien-Ball, J. McBride, D. Klenerman, and S.J. Davis. 2021. Trapping or slowing the diffusion of T cell receptors at close contacts initiates T cell signaling. *Proc. Natl. Acad. Sci. U. S. A.* 118.
145. Bachmann, M.F., K. Mckall-faienza, R. Schmits, D. Bouchard, J. Beach, D.E. Speiser, T.W. Mak, and P.S. Ohashi. 1997. Distinct Roles for LFA-1 and CD28 during Activation of Naive T Cells : Adhesion versus Costimulation. 7:549–557.
146. Grakoui, A., S.K. Bromley, C. Sumen, M.M. Davis, A.S. Shaw, P.M. Allen, and M.L. Dustin. 1999. The Immunological Synapse : A Molecular Machine Controlling T Cell Activation. *Science (80-.).* 285:221–228.
147. Kulenkampff, K., A.H. Lippert, J. McColl, A.M. Santos, A. Ponjavic, S.F. Lee, S.J. Davis, and D. Klenerman. 2019. The costs of close contacts: Visualizing the energy landscape of cell contacts at the nanoscale. *bioRxiv*. 697672.
148. Wild, M.K., A. Cambiaggi, M.H. Brown, E.A. Davies, H. Ohno, T. Saito, and P.A. Van Der Merwe. 1999. Dependence of T cell antigen recognition on the dimensions of an accessory receptor-ligand complex. *J. Exp. Med.* 190:31–41.
149. Burroughs, N.J., and C. Wülfing. 2002. Differential segregation in a cell-cell contact interface: The dynamics of the immunological synapse. *Biophys. J.* 83:1784–1796.
150. Orsello, C.E., D.A. Lauffenburger, and D.A. Hammer. 2001. Molecular properties in cell adhesion: A physical and engineering perspective. *Trends Biotechnol.* 19:310–316.
151. Weikl, T.R., J. Hu, B. Kav, and B. Różycki. 2019. Binding and segregation of proteins in membrane adhesion: theory, modeling, and simulations. *Adv. Biomembr. Lipid Self-Assembly*. 30:159–194.

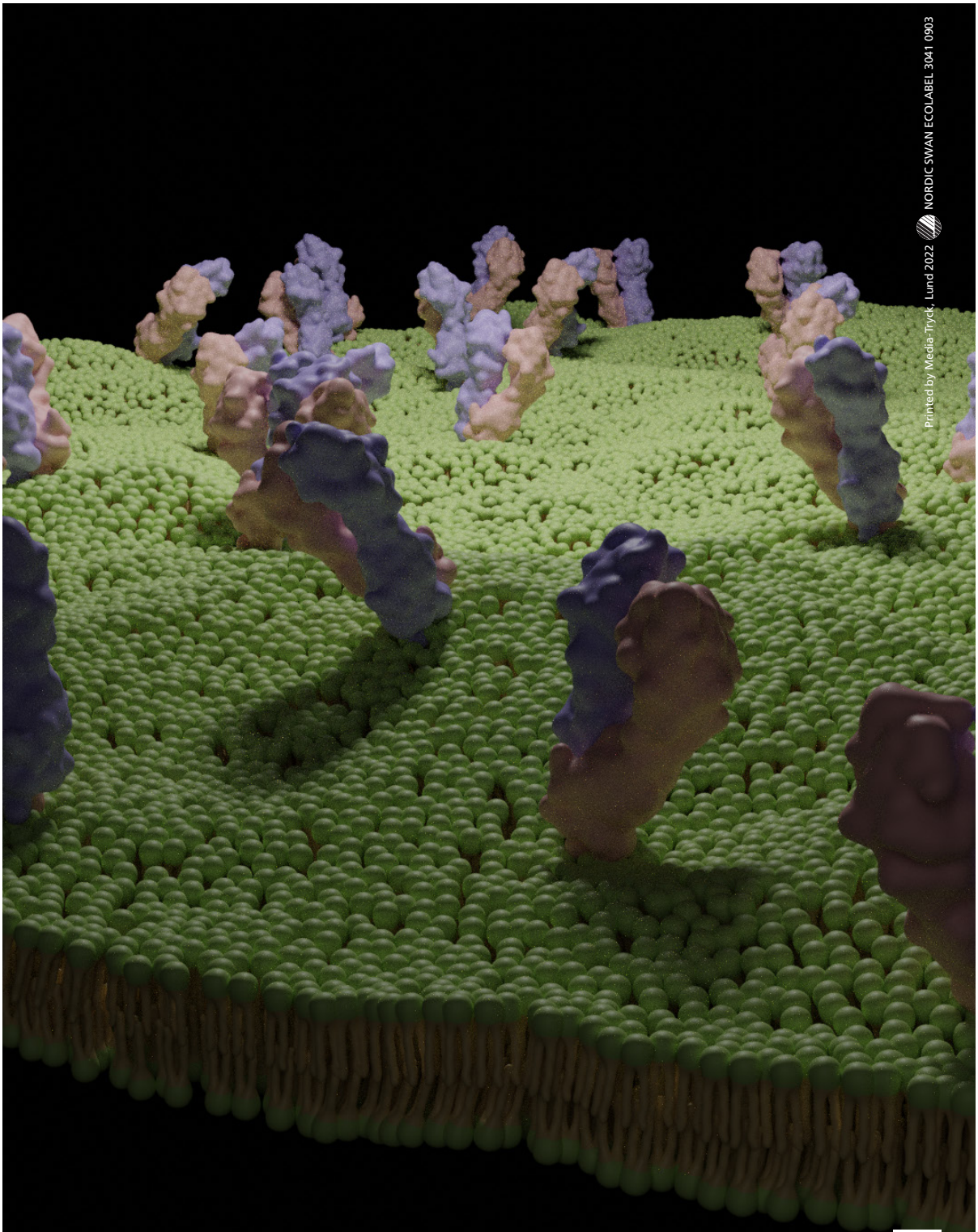

Printed by Media-Tryck, Lund 2022 NORDIC SWAN ECOLABEL 3041 0903

LUND UNIVERSITY

ISBN: 978-91-7422-920-2

Physical Chemistry
Faculty of Science
Lund University